DE TTK

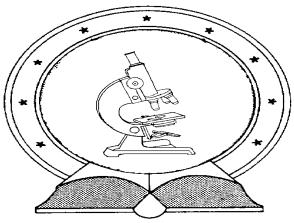

1949

COLLISION INDUCED DISSOCIATION STUDY OF POLYETHERS

Ph.D dissertation

Ghazaleh Shemirani

Supervisor:

Prof. Sándor Kéki, Ph.D., D.Sc.

Debrecen University

Doctoral Council of Natural Sciences

Doctoral School of Chemistry

Debrecen, 2015

Hereby I declare that I prepared this thesis within the program of Debrecen University, Doctoral Council of Natural Sciences, Doctoral School of Macromolecular and surface chemistry K/4 in order to obtain a PhD Degree in Natural Sciences at Debrecen University. The results published in the thesis are not reported in any other PhD theses.

Debrecen, 2015. December. 1. *signature of the candidate*

Hereby I confirm that Shemirani Ghazaleh candidate conducted her studies with my supervision within the K/4 Doctoral Program of the Doctoral School of Macromolecular and surface chemistry between 2010 and 2013. The independent studies and research work of the candidate significantly contributed to the results published in the thesis.
I also declare that the results published in the thesis are not reported in any other theses.
I support the acceptance of the thesis.

Debrecen, 2015. December. 1. *signature of the supervisor*

COLLISION INDUCED DISSOCIATION STUDY OF

POLYETHERS

Doctoral Thesis in order to obtain a Ph.D. degree in the field of Chemistry

Author: **Shemirani Ghazaleh** certified Chemist

Debrecen University, Doctoral School of Chemistry
(Macromolecular and surface chemistry Program)

Supervisor: **Dr. Kéki Sándor**

Comprehensive Examination Committee:

Chair:	Dr. Sóvágó Imre
Members:	Dr. Posta József
	Dr. Csiszár Emília

Date of Comprehensive Examination: 2015. September. 11.

Opponents of the Thesis:

	Dr.	.....
	Dr.	.....
	Dr.	.....

Opponent Committee:

Chair:	Dr.	.....
Members:	Dr.	.....
	Dr.	.....
	Dr.	.....
	Dr.	.....

Date of the defense of the thesis: 2016

ACKNOWLEDGEMENTS

This dissertation would not have been possible without the guidance and the help of several individuals and contributors and their valuable assistance in preparation and completion of this study.

First and foremost I want to thank my initial advisor Prof. László Muszbek and my advisor Prof. Sándor Kéki. It has been an honor to be their Ph.D student. Their precious support from the initial to the final level encouraged me to complete my researches.

I am thankful to the all members of the Clinical Research Center and Chemistry Department for their helpful career advices and suggestions during this work.

I would like to give special thanks to Dr. Ákos Kuki, Dr. Lajos Nagy, and Dr. Eszter Tóth because of their selfless help.

Last but not least I wish to express my deepest gratitude and love to my beloved family specially my brother, Dr. Amir Houshang Shemirani, for their support, strength, help and for everything.

“A few years ago the idea of making proteins or polymers “fly” by electrospray ionization (ESI) seemed as improbable as a flying elephant, but today it is a standard part of modern mass spectrometers”

Professor Fenn in his Nobel lecture

1. ABBREVIATIONS

APCI	atmospheric pressure chemical ionization
APPI	atmospheric pressure photoionization
CAD	collision-activated dissociation
CE	capillary electrophoresis
CI	chemical ionization
CID	collision induced dissociation
CRM	charged residue model
DART	direct analysis in real time
DETA	diethylenetriamine
DOF	degrees of freedom
EI	electron ionization
ESI	electrospray ionization
ETD	electron transfer dissociation
FAB	fast atom bombardment
FTICR	fourier transform ion cyclotron resonance
HPLC	high performance liquid chromatography
IEM	ion evaporation model
IRMPD	infrared multiphoton dissociation
ISCID	in-source collision-induced dissociation
LC	liquid chromatography
MALDI	matrix-assisted laser desorption ionization
MCP	microchannel plate

MRM	multiple reaction monitoring
MS	mass spectrometry
MS/MS	tandem mass spectrometry
NaTFA	sodium trifluoroacetate
PEG	polyethylene glycol
PPG	polypropylene glycol
PTHF	polytetrahydrofurane
PTMG	poly (tetra methylene glycols)
PTMO	poly (tetra-methylene oxides)
QIT	quadrupole ion traps
Qq-TOF	quadrupole-time-of-flight
RF	radio frequency
ROP	ring-opening polymerization
RRK	Rice–Ramsperger–Kassel
RRKM	Rice–Ramsperger–Kassel–Marcus
SIM	selected ion monitoring
SY	survival yield
TOF	time of flight

2. INTRODUCTION

2. 1. Mass spectrometry

Mass Spectrometry (MS) were born in UK in 1897 by J. J. Thomson, a British physicist, who discovered the electron and its m/z ratio [1]. In 1918 A. J. Dempster developed what is considered the first modern mass spectrometer [2]. MS has played important role in many fields of sciences such as, polymer, environmental studies, inorganic applications, etc. [1, 3]. Application of mass spectrometry is not limited to chemistry and physics. It has powerful application in biology, pharmacy and medicine as well. Some examples are direct analysis of intact proteins, drug metabolism, lipid analysis, metabolomics, quantitative proteomics, and imaging of both small molecules and proteins in tissues [4]. Mass spectrometry has had a long story and was applied as a sensitive analytical method for the structural characterization of molecules from long time ago [5].

Harold Wiley well said the truly definition of mass spectrometry, in 1949: "About the best, short, non-technical description of the mass spectrometer is that it weighs molecules, sorts them according to weight, then counts the number of each weight". In a more technical sense mass spectrometry is a method which determines the mass of a molecule by measurement of mass-to-charge ratios of the ions formed when a sample is ionized. The ions are separated, and detected so that the information of the molecular mass and molecule structure can be reached.

All mass spectrometers contain the following parts (Fig. 1). Introducing inlet e.g. a chromatograph, ion source to generate ions from the sample, mass analyzer to separate the ions based on their mass-to-charge ratio, detector to count the ions and measure their abundance and recorder to process the data [1]. Most of the ions are reactive and short lived in the gas phase.

For mass spectrometer working, in most cases, the mass analyzer and the detector must be kept under high vacuum condition of 10^{-6}-10^{-7} torr by turbo molecular pump or diffusion pump [5, 6].

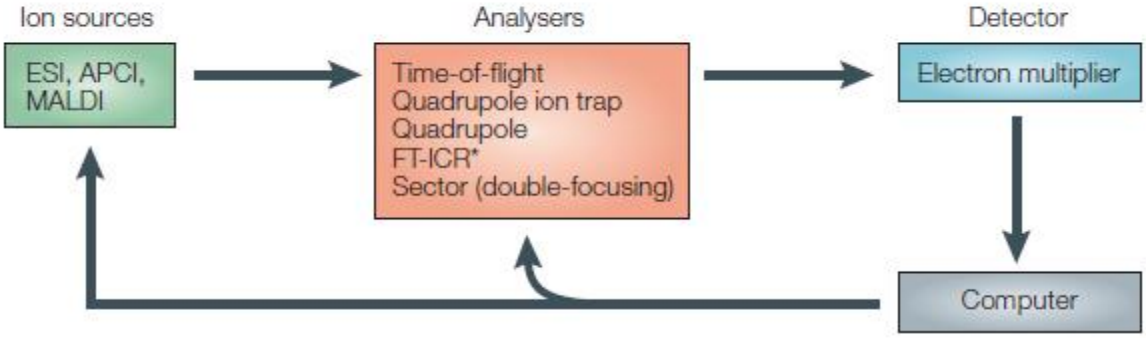

Fig. 1. Basic diagram for a mass spectrometer [7].

The mass spectrometry is based on the analysis of ionized molecules of a sample [8]. The ions can form in many different ways:

$M + e^- \rightarrow M^{+\cdot} + 2e^-$ removing an electron

$M + e^- \rightarrow M^{-\cdot}$ adding an electron

$M + X^+ \rightarrow (M + H)^+$ adding positively charged species (H^+)

$M - X^+ \rightarrow (M - H)^-$ removing positively charged species (H^+)

A mass spectrum shows the relative abundances of ions made in an ion source as a function of their mass to charge ratios [9].

There are two questions that are expected be answered by MS for every sample: what the sample contains? and how much? Sensitivity (limit of detection) and selectivity (absence of interference of other components) are two important words to describe the mass spectrometer methods [10].

There are different ways to introduce sample to the ionization part, some of them are: direct infusion, gas chromatography, high performance liquid chromatography (HPLC) and capillary electrophoresis (CE). Depending on the type of the ion source, we used different type of sample introduction e.g. CE or HPLC are coupled by electrospray ionization (ESI) [11].

In ion-sources, samples are ionized. In this part the analytes of interest are converted into gas phase ions. Generally, this conversion occurs in two steps: first the sample is volatilized, second it is ionized [7]. There are two types of ionization, soft ionization e.g. Chemical Ionization (CI) and hard ionization e.g. Electron Ionization (EI). The ions are formed by CI have little excess of internal energy to induce fragmentation in the mass spectrum and molecular species can be recognized easily. Hard ionization gives us a spectrum contains lots of fragmentations according to the excess ionization energy transferred to the molecule in this method. ESI and matrix assisted laser desorption ionization (MALDI) are two examples of ion sources are used in soft ionization most frequently, for the analysis of non-volatile and thermally labile compounds [1, 7].

There are other types of ion sources: Atmospheric pressure chemical ionization (APCI), atmospheric pressure photoionization (APPI), direct analysis in real time (DART), Fast atom bombardment (FAB), etc. [7].

2. 2. Electrospray ionization (ESI)

ESI is a soft ionization technique that produces ions in gas phase (none or minimal fragmentation) at atmospheric pressure [5]. Electrospray works in both positive or negative ion modes [12]. There was always a problem with measuring the proteins masses with high molecular weight till Fenn has changed the world of mass spectrometry by introducing ESI in 1989. Before that time the analysis of the protein needs its digestion but ESI can analyze the

intact chemical species e.g. proteins [5]. In addition, ESI can analyze synthetic polymers, nucleic acids and molecules with both acidic and basic functional groups [5]. ESI-MS can also scale the analytes including polar organic [13], inorganic [14] and metal-organic complexes [15]. In ESI, the internal energy of the analyte is low, there is no considerate fragmentation upon ionization and very weak non-covalent interactions are conserved in the gas phase [5, 16].

In ESI, the analyte solution undergoes three important processes to be transferred to the gas phase. 1. the charged droplets forming from the high-voltage capillary tip, 2. evaporation of solvent from the charged droplet that results the charged analyte, 3. forming gas-phase ion. The details of the processes are explained bellow.

A dilute analyte solution under atmospheric pressure is injected to a high electric field by syringe pump through the needle or stainless steel capillary (0.2 mm outer diameter, 0.1 mm inner diameter) at constant low flow rate (typically 1-20 μL/min). This high voltage disperses the solution into the highly charged droplets (Fig. 2) [5]. Solvent evaporation by heating or dry gas (N_2) causes the droplets become smaller [17]. Finally, the surface tension cannot tolerate the Coulomb repulsion (repulsion force between the same charges on the surface) and the parent droplet splits into smaller offspring droplets. This phenomenon is called Coulomb fission. The offspring droplets have almost 2% mass and 15% charge of their parent droplets [18]. The evaporation and Coulomb fission repeat to generate smaller and smaller offspring droplets in order to form the gas-phase charged analyte molecule [18, 19]. Some droplets pass through the sampling cone or the heated capillary (0.2 mm i.d, 60 mm in length, and heated to 100-300^{o}C). The droplets become desolvated and transformed through the capillary so this relatively low internal energy ions enter into the mass spectrometer [5]. Electrospray usually produces multiply charged ions so the spectra represent the different charge states of the same molecular species

[20, 21]. By increasing charge the mass to charge ratio (m/z) is decreased. That is why the identification of high mass species can be achieved by mass analyzer with limited (m/z) range [22]. ESI is mostly used in the case of polar compounds and trough adduct ion formations. Neutral ones can be converted to ionic form by protonation or cationization (positive ion mode) and deprotonation (negative ion mode) [17].

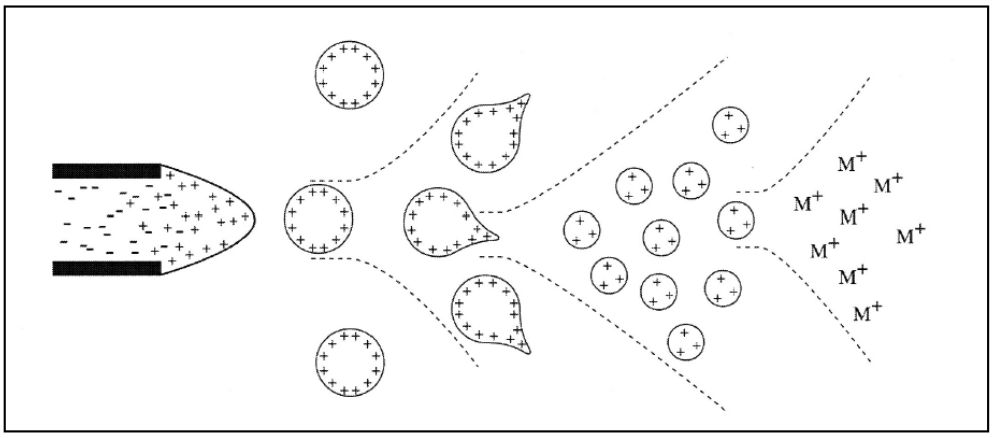

Fig. 2. The schematic of ESI function [17].

There are two basic mechanisms in ESI gas phase ion formation: the charged residue model (CRM) and the ion evaporation model (IEM) [23]. The former model (Dole, 1968) suggests that the electrospray droplets undergo evaporation and breakdown cycles. Multitude of much smaller daughter droplets formed from every initial droplet. Each final daughter droplet contains only one molecule of analyte. When the solvent molecules totally evaporate from such droplet the analyte molecule is left with the charges carried by droplet. The latter model (Iribarne and Thomson, 1976) suggests that droplets become smaller by evaporation until the field strength at their surface is high enough to remove the solvated ions. When the ion is expelled

energy is needed to escape from the surface of the droplet. The strong electric field at the surface of the droplet provides that required energy [24].

Fig. 3 shows the general shape of ESI mass spectrum. The peaks represent the intact molecule spices with variable charging (in case of pure analyte solution). The highest peak with sign of (n^+) and 100% relative abundance is called base peak [5].

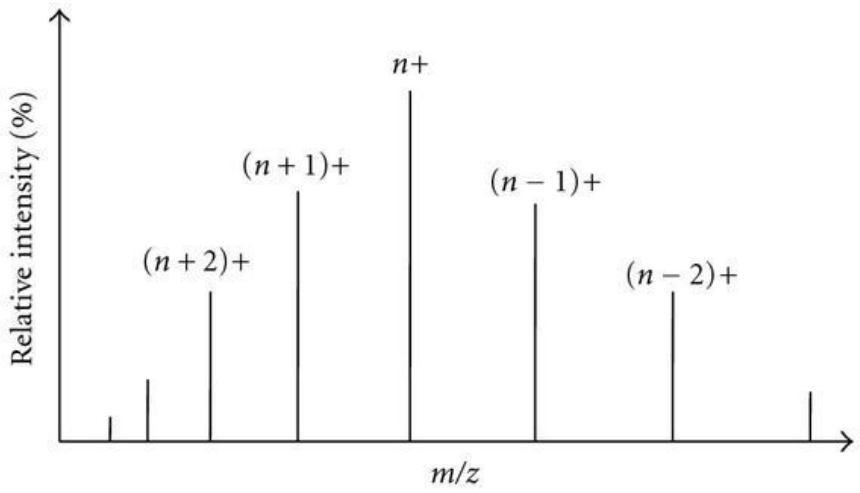

Fig. 3. A typical cartoon representing the nature of ESI-mass spectrum in positive ion mode [5].

Mass analyzers

In mass analyzers the ions are analyzed and separated according to their m/z ratio by magnetic or electric fields [1]. There are different types of mass analyzers. Although we know there are some limitations for any type, choosing one of them depends on its application, performance desired and cost [21]. Some important factors in MS are: mass accuracy, mass range, linear dynamic range and resolution ($m/\Delta m$) where m is the mass of the peaks are resolved and Δm is the mass difference between the two adjacent peaks. Some types of mass analyzers are listed below [21]:

Quadrupole (Q): is used as a mass filter for scanning procedure by changing DC (direct current) and RF (radio frequency) voltage, time of flight (TOF): measure the time is needed for moving accelerated ions from ion source to the detector through a field-free flight tube. The time is correlated to the ion masses, quadrupole ion traps (QIT): qualitative anlyzer in which the trapped ions can be activated and manipulated by RF voltage for mass scanning [25], fourier transform ion cyclotron resonance (FTICR): determine the ion masses by measuring the cyclotron frequency of circular moving ions. The frequency is dependent on ion masses, and magnetic sector: deflected ions to a circular movement be accelerated to a high velocity and be separated based on their m/z ratio by applied magnetic field in the magnetic sector. Quadrupole and TOF mass analyzers are coupled with ESI in our mass spectrometric experiments to perform tandem mass spectrometric investigations. So it is a right place to mention some details of their structures.

2. 3. Quadrupole mass analyzer (Q)

Every quadrupole are composed of four parallel metal rods (Fig. 4). RF voltage is applied between each opposing rod pair. The RF voltage is covered by a DC voltage [1]. By changing DC and RF potentials only one specific m/z at a time can pass the quadrupole and reach the detector. Others are neutralized by colliding with the roads [26-28]. Quadrupole can measure the m/z of the negative ions as well. Single ion monitoring (SIM) is an important analysis mode. This mode increases the sensitivity by decreasing the signals came from other chemical ions rather than from the compound of interest. In this method mass analyzer is set to monitor the intensity of specific single m/z value instead of the full mass spectrum.

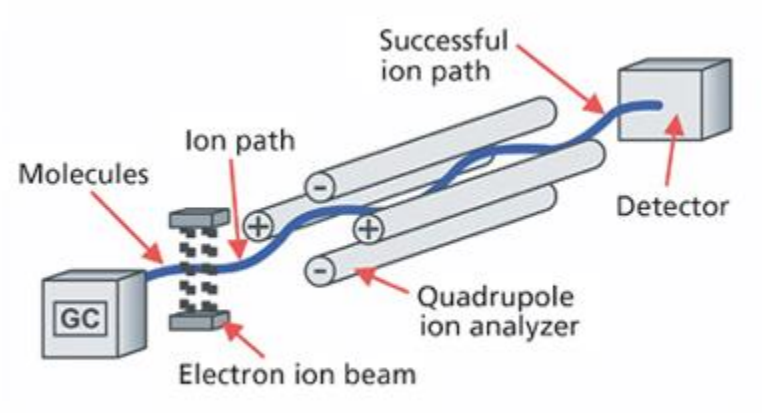

Fig. 4. Diagram of a quadrupole mass analyzer [26].

2. 4. Time of flight mass analyzer (TOF)

TOF analyzers accelerate the ions by applying voltage gradient and measure the time is needed for moving ions of different masses through a field-free flight tube. The flight time is proportional to the square root of the m/z ratio [29]. It is shown in Eq (4). The kinetic energy of an ion (E) leaving the ion source is:

$$E = \frac{mv^2}{2} = qU, \qquad q = ze \tag{1}$$

where m is mass of the ion, v is ion velocity, q is the charge, z is number of charges, e is charge of an electron and U is acceleration voltage. Eq (2) shows the relation between ion velocity, length of the flight path (L) and time of flight (t).

$$v = \frac{L}{t} \tag{2}$$

substation of Eq (1) into Eq (2), Eq (3) comes as:

$$m = \frac{2qUt^2}{L^2} \tag{3}$$

by rearranging Eq (3) reach to the time of flight in Eq (4).

$$t = L\sqrt{\frac{m}{2qU}} \quad (4)$$

TOF can reach resolution of 10,000 or higher [30]. This analyzer has linear and reflector modes, in linear mode high masses molecules are measured and in reflector mode all ions are reaccelerate to increase the resolution [31]. Ions reach to the analyzer have neither the same kinetic energies nor the same starting times. Reflectron lets ions with a higher initial kinetic energies penetrate deeper and spend more time there, therefore it takes longer time that ions with more kinetic energies reach the detector. With reflectron, the ions with the same m/z can reach the detector at the same time, regardless of their initial kinetic energies (Fig. 5). This mode increases the mass accuracy and resolution of TOF. Up to several hundred thousand mass of ions can be measured by TOF instrument [7].

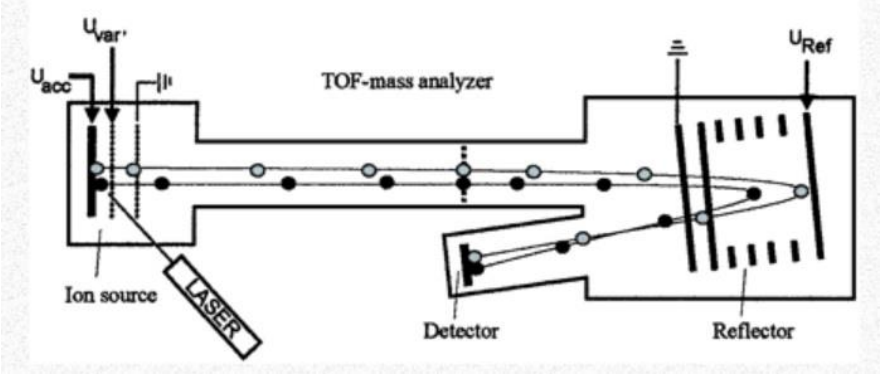

Fig. 5. TOF mass analyzer [32].

Detectors

Ions formed in ion source, passed and separated through mass analyzer should be electrically detected by an appropriate detector to identify the number of ions for each mass produced [6]. There are some properties for desirable detectors like high amplification, low

noise, low cost, fast time response, narrow responses distribution, high efficiency, long term stability, etc. [33].

Microchannel plate (MCP) is the detector that is used in our ESI instrument. A MCP is an array of 10^4-10^7 tiny electron multipliers oriented parallel to each other (fig. 6), channel diameters are in the range 10-100 μm and have length to diameter ratios (α) between 40 and 100. Channel axes are biased at a small angle (~8°) to the MCP input surface. The channel matrix is made of a lead glass in order to optimize the secondary emission features of each channel and to reduce the semiconducting characteristic of channel walls. In this situation walls allow charge refill from an external voltage source. Thus each channel works as its own dynode resistor chain. Deposition of a metallic coating on the front and back surfaces of the MCP (input and output electrodes) provides the parallel electrical contact to each channel. The channel dimensions are typically 12 μm diameter channels with 15 μm center-to-center spacing [34]. Many authors have sufficiently covered the theory of channel multiplication [35-37].

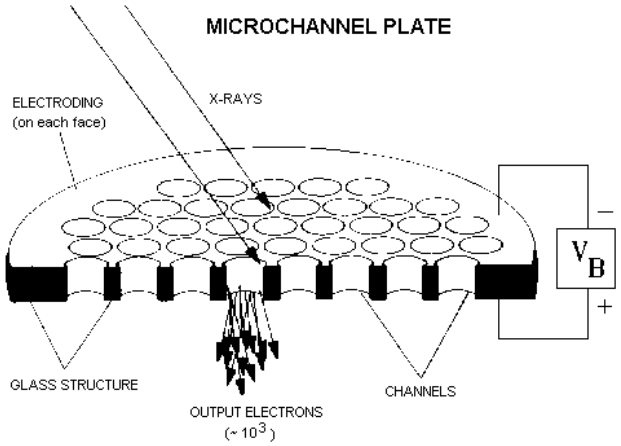

Fig. 6. Microchannel plate (MCP) detector [34].

Tandem mass spectrometry (MS/MS)

Very important information about the structures of the molecule can be obtained by tandem mass spectrometry [5]. The result of single MS spectrum may include lots of product ions that may not related to the compound of interest. With this abundance the prediction of the structural information of the compound would be difficult. It was necessary to find a way to select some ions are produced in the source in order to fragment them selectively and to analyze their fragments. Tandem mass spectrometry (MS/MS) techniques develop that way [38].

The simple definition of MS/MS is a two-step of MS. In the first stage, the ions with chosen m/z ratios are selected from the other product ions [39]. Then, these parent or precursor ions will be activated in order to increase the internal energy of those ions to be fragmented.

After chromatography separations, triple quadrupole mass spectrometer usually measure the amounts of some certain samples in the mixtures by tandem mass spectrometry. The first quadrupole (Q1) is a scanner and selects the ion to be fragmented, so only the mass of the desired precursor ion will be transmitted through this quadrupole. Second quadrupole (Q2) is a collision cell, the selected parent ions collide with argon, xenon or nitrogen and be fragmented into several product ions. In the third quadrupole (Q3) only a selected daughter ion formed by fragmentation of the parent ion will be transmitted to the detector [40].

There are four different scan modes in triple quadrupole MS/MS technique [39]. The first one is neutral-loss scan. In this scan mode the first stage of MS (MS-I) and the second stage (MS-II) are offset by desired neutral mass that is lost or gained during the reaction between two steps of MS, while both of MS stages are scanned. The (Q3) scans the mass range according to the offset to (Q1). Ions that have lost a fragment with the mass according to the offset will be passed to the detector [31]. The second one is precursor-ion scan. In this scan mode MS-I is scanned and set to pass all the ions that released from ion source but the MS-II is set on a

specific m/z. (Q3) is set to the specific mass of fragmented ion that can reach the detector (Fig. 7). The third mode is the product ion scan in which a definite precursor ion is selected by MS-I while MS-II scans through a specific mass range [39]. The last quantitative MS/MS method is SRM (single reaction monitoring) and MRM (multiple reaction monitoring). If there is a single parent and product ion it will be a SRM experiment. MRM is a mode that is set typically for the measurement of e.g. complex biological samples. It has two forms, in the first form the single parent ion pass through the first MS stage and two or more known product ions are transferred through MS-II. The other form of MRM includes multiple parent ions [7].

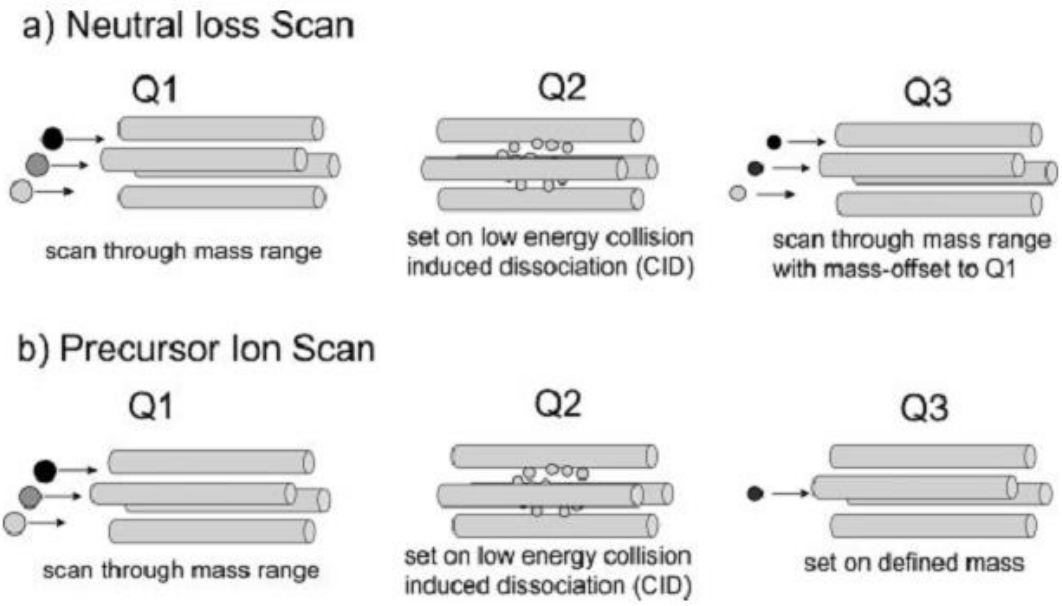

Fig. 7. Schematic illustration of a neutral loss scan (a) and a precursor ion scan (b) [31].

The quadrupole-time-of-flight (Qq-TOF) mass spectrometer is the same as a triple quadrupole but in the former the third quadrupole is replaced by a TOF analyzer. Qq-TOF is more sensitive compared with triple quadrupole because its duty cycle is lower [41]. Duty cycle is a fraction of time in which ions delivered from ion source to analyzer [42].

Ion activation methods

The activation practically is not separated from dissociation. There are several ways for ion activation such as surface-induced dissociation (SID), electron capture dissociation (ECD) [7, 39], electron transfer dissociation (ETD) and infrared multiphoton dissociation (IRMPD) [43]. One of the commonly used activation method to activate the selected ions in tandem mass spectrometry is collision-activated dissociation (CAD) or collision-induced dissociation (CID) [39, 44].

Electron capture dissociation (ECD) is a method in which the thermal electrons react with molecules in a mass spectrometer. An analyte molecule captures a low energy electron and produces negative ions. This process happens under high pressure conditions. $M^{-\cdot}$ shows the odd-electron negative ion. ECD results are:

Resonance electron capture: $AB + e^- \rightarrow AB^{-\cdot}$

Dissociative electron capture: $AB + e^- \rightarrow A^{\cdot} + B^-$

Ion-pair formation that results from electron capture: $AB + e^- \rightarrow A^- + B^+ + e$ [45].

CID process takes place in two steps. The first one is the excitation of the precursor ions, the second part is a unimolecular dissociation of an excited ion and separation of the fragment (product) ions [46]. In this method the precursor ions collide with the neutral target gases like N_2, Ar, Xe or He (collision gases). This collision causes the energy is gained by precursor ion and distributed between different vibrational degrees of freedom [5]. This extra energy causes the precursor ion to decompose into the product ions in CID unimolecular fragmentation process. These product ions will be analyzed by the second stage of MS/MS [7, 39]. One of the most important effective factors on characterizing the energetics of fragmentations in CID is survival yield curve (SY). SY is a plot of relative ion intensity ratios of the precursor ion to those

of all product ions in which the precursor ion is a function of the collision energy (Eq. 5) [47-49].

$$SY = \frac{I_p}{I_p + \sum I_{F,i}} \quad (5)$$

where I_P is the intensity of the precursor ion, and $\boldsymbol{\Sigma} I_{F,i}$ is the sum of all fragment ion intensities.

The rate constant of unimolecular reactions $k(E_{int})$ occurring in a mass spectrometer can be calculated by the original Rice-Ramsperger-Kassel (RRK) model (Eq. 6).

$$k(E_{int}) = A\left(1 - \frac{E_0}{E_{int}}\right)^{S-1} \quad (6)$$

where A is the pre-exponential factor, E_o is the critical energy for fragmentation, E_{int} is the internal energy of the ion and S is the total degrees of freedom (DOF). More sophisticated Rice-Ramsperger-Kassel-Marcus (RRKM) formalism (Eq. 7) also gives the comparable results with those of the RRK when the DOF is reduced to about one-fifth in RRK formalism [50].

$$k(E_{int}) = \frac{\sigma W^{\neq}(E_{int} - E_0)}{h\rho(E_{int})} \quad (7)$$

where σ is the reaction path degeneracy, $W^{\neq}(E_{int}\text{-}E_o)$ is the sum of states of the transition state, h is the Planck's constant and $\rho(E_{int})$ is the density of states of the reactant.

There are other different factors that affect the CID such as single or multiple collisions with a selected gas, the relative translational energy of the ion and the gas molecules, the nature of the selected gas, etc. Distribution of internal energy of activated ion is influenced by these factors [39, 44]. An inelastic collision between a high translational (kinetic) energy ion and neutral gas molecules causes a part of the translational energy is changed into E_{int}, leading to the decomposition. Center of mass collision energy (E_{com}) is the maximum amount of the energy that can be converted into internal energy of the precursor ion in a single collision, practically in a totally inelastic collision (Eq. 8).

$$E_{com} = \left(\frac{m_g}{m_p+m_g}\right)E_{kin} \quad (8)$$

where m_g and m_p are the mass of the collision gas and mass of the precursor ion, respectively and E_{kin} is the kinetic energy (in the lab frame) [46]. There is no internal energy transfer in totally elastic collision. The increase in the internal energy of the ion in the first collision ($\Delta E_{int,1}$) is related to E_{com} as given by Eq (9).

$$\Delta E_{int,1} = \eta E_{com} \quad (9)$$

where η is the collision inelasticity, i.e., the fraction of center-of-mass energy transferred to internal energy in a single collision. η is usually changed between 0-1 and it is maximum when the collision is totally inelastic [51].

As seen in Eq (8), higher mass of precursor ions have lower internal energy for fragmentation during the collision procedure [46, 52]. The experiment can be performed at high or low collision energy in different mass analyzers like time of flight or tandem quadrupole, respectively [39]. The high-energy CID spectrum is more complicated than low-energy spectrum, but it contains more structural information as well.

2. 5. Polyethers

Simply, polyether is a kind of polymer consisting of ether bonds in the backbone (an oxygen atom connected to two alkyl or aryl groups): R–O–R' (Fig. 8).

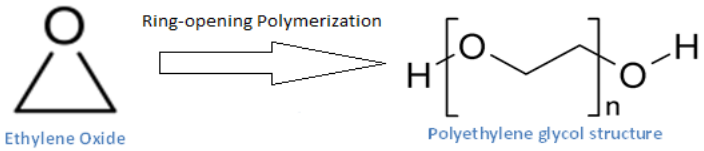

Fig. 8. Schematic of PEG polymerization.

Since our work was on polyethers such as Poly(ethylene glycol) (PEG) or poly(ethylene oxide) (PEO), poly(propylene glycol) (PPG) or poly(propylene oxide) PPO, poly(tetrahydrofuran) (PTHF) or poly(tetra-methylene oxides) (PTMO) or poly(tetramethylene glycols) (PTMG) and diethylentriamine (DETA) polyols (Scheme. 1), it is good place to mention some properties and applications of them.

PEGs, PPGs and PTHFs are prepared by ring-opening polymerization (ROP) of ethylene oxide, propylene oxide and tetrahydrofuran, respectively. These polyethers can be solid or liquid depending on their molecular weight [53, 54].

Polyether glycols, also known as polyoxyalkylene glycols, include wide variety of polymeric materials with molecular weights ranging up to 100,000 molecular mass and above. These polyethers have different applications in different areas such as making plastic products, production of polyurethane, vehicles, solvents, chemical intermediates in the rubber, pharmaceutical products carrying out pegilation process, agricultural, textile, paper, petroleum and other industries. Some derivatives of these materials, by physical and chemical properties modification, also have a large variety of applications [55]. One of the most important roles of PEG, PPG, PTHF and their copolymers is their application in medicine [56-61].

PEG can be utilized as thermal energy storage and this character makes it usable in industrial heat utilization, electronic device management and protection [62]. It is also used as lubricant fluid in compressors. Its high biocompatibility makes it a good choice to use in cosmetic and pharmaceutical products [63]. Addition of PEG and PVA (Poly Vinyl Acetate) to ethylcellulose pallet coating causes drug release within 8-12 h, irrespective of the compound of pallet core [64]. PEG-β-cyclodextrin is used for preparation of hydrogel because of the tunable properties and good biocompatibility. Hydrogel applied in drug delivery system, medical devices and tissue engineering [65]. PEG enhances the dehydrochlorination of PVC and it is

environmentally friendly because some waste plastic containing PVC can be dehyrochlorinated with high efficiency by PEG [66]. PEG-coated gold nanoparticles may have important clinical implications as they are widely used in biomedical applications [67]. This polymer can obstruct pulmonary dysfunction with the support of endothelial cells in injured lung tissue [68].

PPG is used in many formulations for polyurethane. Secondary hydroxyl group in PPG is less reactive than primary OH group in PEG. PPG with 1200 Da molecular weight is a biocompatible solvent with the high partition coefficient for butanol. This special character applies in fermentation experiments [69]. It is used in some organic synthesis for instance star-shaped polymer prepared by coordination of 2,2'-bipyridyl-terminated poly (propylene glycol). It is soluble in water and some organic solvents [70]. Isolated bacteria can grow on PPG and PEG and on their dehydrogenases [71].

The five arm star diethylenetriamine (DETA) polyol is from the family of aliphatic amine PPG polyols. It is used for producing the rigid polyurethane foams for thermal insulation. Reaction of DETA, which has five initiation sites, with propylene oxide, forming presumably a five arm star structure [72].

Some characteristics of PTHF are dynamic mechanical properties across a wide temperature range, exceptional low temperature behavior, excellent abrasion resistance and superior hydrolytic stability. These properties cause that PTHF is widely used by industry [73]. This polymer is utilized in many materials as the soft segments. Two examples are polyurethane and polyamide based thermoplastic elastomers [74]. Many bio-resistant and biocompatible thermoplastic polyurethane elastomers targeted at various biomedical applications contain PTHFs [75-78]. The application of PTHFs will increase in future [79].

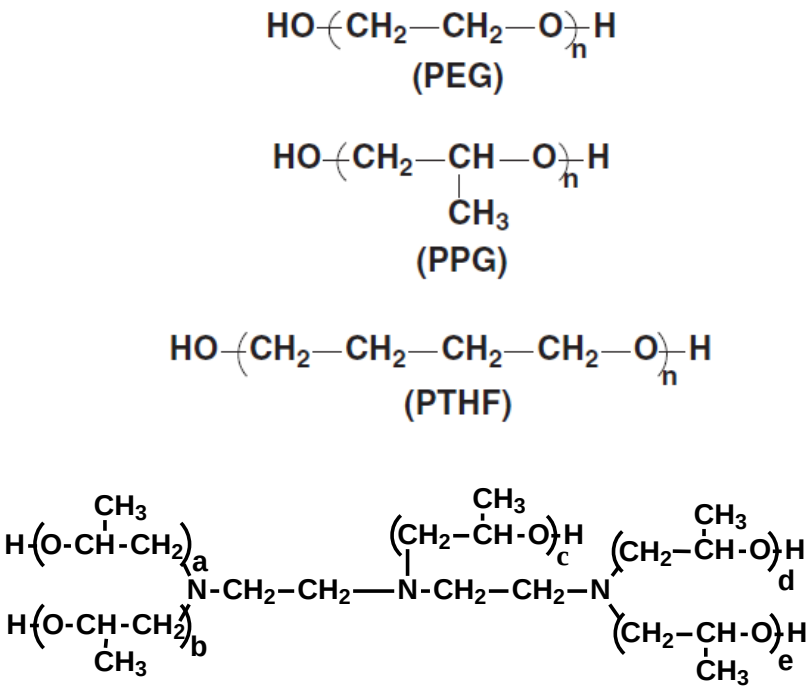

Scheme. 1. The structure of PEG, PPG, PTHF, and DETA [72, 80].

3. AIMS

1. It was found that the dominant, and almost unique, process in the MS/MS of the doubly cationized polyethers (PEG, PPG, and PTHF) was the simple loss of a cation from the doubly charged precursor to yield the singly charged product ion.

2. It was observed that the collision voltage necessary to obtain 50% fragmentation (CV_{50}) determined for the doubly cationized polyethers increases linearly with the size or degrees of freedom (DOF) for each polyether studied.

3. The slopes of the CV_{50} versus DOF curves were correlated with the relative gas-phase dissociation energies for binding of alkali ions to polyethers. The relative dissociation energies determined from the corresponding slopes were found to decrease in the order $Na^+ > K^+ > Cs^+$ for each polyether studied, and an order PPG ≈ PEG> PTHF can be established for each alkali metal ion.

4. A simple collision model for treating the multiple collisions taking place in quadrupole (Q) type mass spectrometers has been developed. This model is capable of calculating the internal energy increment, the transit time and the exit energy of the ions in Q-type mass spectrometers. The calculations showed that there were good agreements between the results obtained by our model and the SIMION simulation. Implementation of the collision model and RRKM or RRK algorithm into a spreadsheet software allowed a good fitting of the calculated data to the experimental survival yield (SY) versus collision energy curve.

5. The collision model with the RRKM formalism was used to estimate the efficiencies of the kinetic to internal energy conversion for leucine enkephalin in quadrupole-time-of-flight and triple quadrupole instruments. It was found that reducing the total degree of freedom (DOF)

to about one fifth in RRK formalism, the RRK can give comparable results with those of the more complicated RRKM model.

6. The critical energy (E_o) of lithiated polyethers including PEG, PPG and PTHF with degrees of freedom similar to that of leucine enkephalin was calculated by this collision model with the RRK formalism. Thus, the RRK model could predict the corresponding rate constant with a reasonable accuracy.

7. The collision-induced dissociation of the protonated five-arm star propoxylated diethylenetriamine polyols was studied under electrospray conditions. It was shown that the cleavage of the C-N bonds in the initiator moiety results two product ion series. No backbone fragmentation of the polyether chains was observed.

8. Binomial distribution was proposed for the description of arm-length distribution. The initiation and propagation process of the oligomers was explored. It was concluded: (1) the repeat units attach to the five arms with approximately the same probability, and (2) the reaction rate of the initiation is greater than that of the chain propagation.

9. It was found that there is a linear relationship between the collision energy necessary to obtain 50% fragmentation (CE_{50}) and the number of propylene oxide repeat units.

4. MATERIALS AND METHODS

4. 1. Chemical materials

All chemicals for polyethers experiments were received from Aldrich (Steinheim, Germany). The polyethers were used in estimation of stabilities of cationized polyethers were: PEG with number-average molecular weights of 1000 and 1540 g/mol, PPG with number-average molecular weights of 1000 and 2000 g/mol and PTHF with number-average molecular weights of 650 and 1400 g/mol.

Leucine enkephalin and the polyethers: PTHF with a number-average molecular weight (Mn) of 650 g/mol, PEG with Mn of 400 g/mol and PPG with Mn of 600 g/mol were used for the experiment.

The sample used in diethylenetriamine experiment was of industrial propoxylated diethylenetriamine (Petol PA 500-5D, Scheme 1) with an approximate number average molecular weight of 500 g/mol (Oltchim, Valcea, Romania).

4. 2. Sample preparation

Each polymer was dissolved in methanol at a concentration of 2 mM. To obtain the corresponding adducts of polyethers in ESI, a solution of NaCl or KCl or CsCl in methanol was added to the corresponding polyether solution to obtain 1mM concentration for the polymer and for the alkali metal salt.

In the leucine enkephalin experiment, to obtain lithiated adducts of the polyethers in ESI, a solution of LiCl in methanol was added to the polyether solutions (in methanol) to obtain 1 mM concentration of the polyethers and LiCl. Leucine enkephalin was introduced into the ESI-source in a concentration of 2 ng/μL dissolved in acetonitrile/water-0.1% formic acid (1/1 V/V).

The DETA sample was dissolved in HPLC grade methanol (VWR International, Leuven, Belgium) at a concentration of 0.1 mg/mL.

Electrospray Quadrupole Time-of-Flight MS and MS/MS (ESI-MS and ESI-Q-TOF)

The MS and MS/MS measurements were performed with a MicroTOF-Q type Qq-TOF MS instrument equipped with an ESI source with positive ion mode from Bruker (Bruker Daltonics, Bremen, Germany). The sample solutions were introduced directly into the ESI source with a syringe pump (Cole-Parmer Ins. Co., Vernon Hills, IL, USA) at a flow rate of 3 μL/min. The temperature of the drying gas (N_2) was kept at 180°C. The needle voltage was 4 kV. For MS/MS experiments nitrogen gas was used as the collision gas, and the collision voltages were varied in the range of 10-100 eV for the cationized polyethers experiments and 10-54 eV (in the laboratory frame) for the DETA experiment. The pressure in the collision cell was determined to be 8×10^{-3} mbar. The precursor ions for MS/MS were selected with an isolation width of 2.5, 5 and 4 *m/z* units in different experiments. For MS^3 experiments in-source collision-induced dissociation (ISCID) was applied, the ISCID energy was set to 100 eV. The MS/MS spectra were accumulated and recorded by a digitizer at a sampling rate of 2 GHz. The mass spectra were calibrated externally using the exact masses of clusters $[(NaTFA)_n+Na]^+$ generated from the electrosprayed solution of sodium trifluoroacetate (NaTFA). The mass spectra were evaluated with the Data Analysis 3.4 software from Bruker.

Electrospray Triple Quadrupole MS/MS (ESI-TQ)

Source conditions for the TQ measurements were similar to those of Q-TOF and the measurements were performed with a Finnigan TSQ Quantum triple quadrupole mass spectrometer from Thermo Finnigan (Thermo Finnigan, San Jose, California). For the MS/MS

experiments of leucine enkephalin argon collision gas at pressures of 0.5, 0.7 and 1 mTorr was used. The mass spectra were evaluated with the Xcalibur 2.07 software from Thermo Finnigan.

Determination of the CV_{50} values

The SY was explained before in Eq (5). It should be noted, however, that the cation signal in the case of sodiated and potassiated polyethers could not be observed due to the low mass of these cations (the lowest mass limit on our Q-TOF mass analyzer is m/z 50). Thus to obtain SY values for the cesiated polyethers similarly to those for sodiated and potassiated ones, the Cs+ signal was not included in calculating their SY values. The shape of the SY versus collision energy (eV) or collision voltage (V) curves is a sigmoid type and was described using a four-parameter sigmoid function according to Eq (10).

$$SY = \frac{a-b}{1+ e^{(CV-c)/d}} + b \qquad (10)$$

where a, b, c and d are constants and CV is the collision voltage, c is the collision voltage/energy necessary to obtain 50% fragmentation (CV_{50}), and d refers to the width of the steepest part of the sigmoid curve.

The CV_{50} values can be obtained by fitting the parameters of the four-parameter sigmoid function (Eq. 10) to the experimental data and the c parameter in Eq (10) refers to the CV_{50} value. A home-made software utilizing the Gauss–Newton–Marquardt procedure was used for determining the parameters of Eq (10) [81]. It should be noted that the CV_{50} values can also be obtained by a linear interpolation between two points falling below and above SY = 0.5. Both methods gave practically the same results of CV_{50} values, the obtained CV_{50} values were within ±1%.

5. RESULTS AND DISCUSSION

5. 1. A simple method to estimate relative stabilities of polyethers cationized by alkali metal ions

In the MALDI and ESI mass spectrometry of polar synthetic polymers containing ether or ester groups cationization by alkali metal ion is a good method for increasing cationization of these polyethers [82, 83]. Homopolymers such as PEG, PPG, and PTHF have the very similar structure and the wide commercial availability with varying size, these characters make these polymers ideal candidates for mass spectrometric investigations. Due to the practical utilities and theoretical interest the cationization properties of polyethers with alkali metal ions have been studied by numerous MALDI and ESI-MS studies [84-89]. Determination of the relative binding affinities of the alkali metal ions to polyethers was the most important subject of these studies. The relative ion abundances have been correlated to the respective relative affinities of cations to polyethers in most of these researches.

There are two ways to have reliable data concerning the gas-phase relative binding energies of cations that can be compared to the theoretical values. First: the relative ion abundances should be corrected, second: solvent-free sample preparation with cationization agents of similar lattice energy should be applied, as recently reported for MALDI technique [87]. Producing gas-phase ions followed by collision-induced dissociation and monitoring the fraction of the undissociated precursor ion as a function of the collision energy is a direct way for the determination of the relative gas-phase binding energies of cations to polyethers. This technique is usually used in combination with guided ion beam mass spectrometry or threshold dissociation methods for the determination of the binding energies of cations to small linear and cyclic ethers [90-94].

In this chapter, the detailed systematic investigation of the dissociation of the doubly charged polyethers involving the simple loss of one cation as a function of the collision energy and chain length was reported. Then, we will show that the collision voltage/collision energy necessary to obtain a 50% (CV_{50}) fragmentation varies linearly with the DOF, or degree of polymerization. Furthermore, the molecular mass for the doubly cationized polyethers PEG, PPG and PTHF and the slope values of the corresponding CV_{50} versus DOF are correlated with the relative dissociation energies.

In order to study the gas-phase dissociation energies for binding of the alkali metal ions Na^+, K^+ and Cs^+ to the polyethers PEG, PPG and PTHF doubly charged polyethers cationized with these metal ions were produced by electrospray and the resulting adduct ions were subjected to collision induced dissociation (CID) as a function of chain length and collision energy.

All of the doubly charged polyethers cationized with Na^+, K^+ and Cs^+ showed no backbone fragmentation and the dominant, and almost unique, process in the MS/MS of these doubly cationized polyethers was the simple loss of a cation from the doubly charged precursor to yield the singly charged product ion. The survival yields as defined above were recorded as a function of the collision energy and the degree of polymerization of polyethers. As an example, Fig. 9 shows the survival yield versus collision voltage for the doubly sodiated PEG ($[PEG + 2Na]^{2+}$) with polymerization degrees (n) of n = 23, 29 and 37.

As seen in Fig. 9 the survival yield curves have sigmoid shapes and can be well described by a four-parameter sigmoid model. In addition, it is also evident from Fig. 9 that the SY versus collision energy (voltage) curves shift to higher collision energies with the increasing size, i.e., with the degree of polymerization. To evaluate the shift of the SY with the size, the CV_{50} values, i.e., the collision voltage needed to obtain a 50% fragmentation, was considered.

Furthermore, instead of using the number of repeat units or the mass, the number of vibrational degrees of freedom was employed in comparison of the CV_{50} values obtained for the different polyethers. From a practical point of view the former two are of interest. However, it is actually the DOF, among which the internal energy gained through CID is distributed, that can more realistically represent the effect of size. This is especially important when one intends to compare the CID properties of polymers with varying mass and compositions of the repeat units.

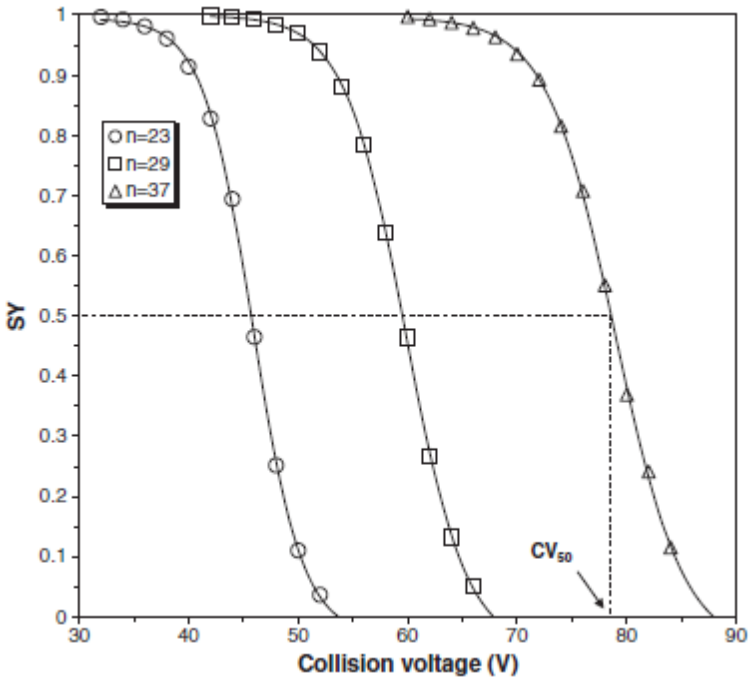

Fig. 9. SY versus collision voltage curves for the doubly sodiated PEG with degrees of polymerization n = 23, 29 and 37. The solid lines represent the fitted curves using the fourparameter sigmoid model. The parameters of these curves are a = 0.99, b = -0.032, c = 45.86 and d = 2.27 for n = 23; a = 0.99, b = -0.056, c = 59.81 and d = 2.78 for n = 29; a = 0.99, b = -0.032, c = 78.94 and d = 3.12 for n = 37.

Fig. 10 reveals the variation of the CV_{50} values with the DOF for the doubly charged polyethers cationized by Na^+, K^+ and Cs^+ ions. Our first observation is that, in the mass range

studied, the CV_{50} values vary linearly with the DOF for all polyethers. It is indicating that the energy needed for the fragmentation increases linearly with the size.

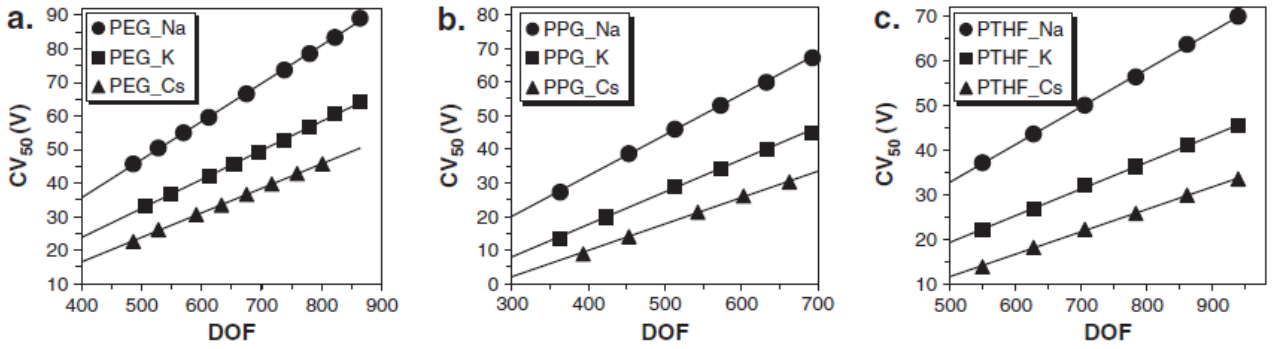

Fig. 10. CV_{50} versus DOF plots for the doubly charged PEG (a), PPG (b) and PTHF (c) cationized with Na^+, K^+ and Cs^+ ions.

The slopes, intercepts and the coefficient of determination (R^2) obtained for the doubly charged polyethers are summarized in Table 1.

According to the data of Table 1, the slopes of the linear trend lines decrease in the order of $Na^+ > K^+ > Cs^+$ for all polyethers. The data in Table 1 show very good linear correlation (R^2 >0.99 in all cases) and support also this conclusion. It is also seen from Table 1 that the slopes of the CV_{50} versus DOF for PEG and PPG are very similar in the case of each alkali metal ion, while for PTHF the slopes are considerably smaller than those for PEG and PPG. Surprisingly, all linear trend lines have considerable negative sign intercepts and the intercepts decrease in the order of $Na^+ > K^+ > Cs^+$.

		Slope		Intercept		Coeff. of det.
Polyether	Cation	value	error	value	error	R^2
PEG	Na^+	0.227	±0.005	-9.693	±1.667	0.9994
	K^+	0.173	±0.003	-10.799	±1.200	0.9995
	Cs^+	0.146	±0.003	-12.730	±0.841	0.9997
PPG	Na^+	0.239	±0.005	-15.755	±1.441	0.9997
	K^+	0.191	±0.010	-20.562	±2.755	0.9985
	Cs^+	0.154	±0.007	-21.011	±2.119	0.9985
PTHF	Na^+	0.169	±0.005	-9.421	±1.791	0.9996
	K^+	0.120	±0.004	-10.607	±1.634	0.9993
	Cs^+	0.101	±0.004	-13.526	±1.387	0.9993

Table 1. Parameters of the fitted linear trend lines determined from the CV_{50} versus DOF/z plots for the doubly charged polyethers. The error values indicated reveal the 95% confidence level.

Estimation of the dissociation energies from the slopes of CV_{50} versus DOF curves

According to the Fig. 10 and Table 1, the linear increase of CV_{50} with DOF, strongly suggests that the decreasing amount of internal energy with the increasing size (mass), i.e., decreasing center of mass energy, is closely compensated by the increased number of collisions due to the increasing collision cross-section. Indeed, ion mobility experiments on singly cationized PEG, PPG and PTHF by Bowers and coworkers have revealed that the cross-sections vary linearly with the degree of polymerization of these polymers [95]. All polyethers studied have practically the same collision cross-section when they are plotted as a function of the number of atoms, i.e., DOF, [95] and this was confirmed more recently by high-level ab initio

calculations. Furthermore, the dynamics of cation detachment must occur with a number of geometrical similarities and hence the pre-exponential factors (that is highly dependent on the structure of the transition state) must have similar values for all of these polyethers and for the various cations. Therefore, it is reasonable to assume that the bond dissociation energies, especially for the larger sized oligomers, remain constant. Thus the slope values may be directly related to the bond dissociation energies. In other words, the higher the slope is the higher the energy needed for fragmentation. This also implies that the bond dissociation energies increase with the increasing slope values.

The gas-phase binding energies of the alkali metal ions to PEG for the singly charged sodiated, potassiated and cesiated PEG have been calculated for oligomers up to the number of repeat units n = 17 using quantum chemical methods [96]. According to these calculations the binding energy of the cation to PEG increases up to n = 10, then it levels off for each cation, indicating that this is the approximate limit of the oligomer size that can be influenced by the alkali cation. The binding energy versus degree of polymerization curves were found to be markedly parallel for the cations and the limiting binding energy of Na^+, K^+ and Cs^+ ions to PEG chains have been calculated to be 4.77, 3.69 and 3.25 eV, respectively. Although there are no similar calculations available for the doubly charged PEG, especially for higher degree of polymerization, it is reasonable to assume that the limiting binding energies are very similar to those of the singly charged ones, though the limiting binding energy may be expected to occur at higher degrees of polymerization for the doubly charged polyethers. In our experiments we used larger-sized polyethers, i.e., PEG oligomers in the range of repeat units (n) 23–41, PPG with n = 12–25 and PTHF with n = 14–24. The strict linearity of the CV_{50}-DOF plots may also suggest that the limiting binding energies of alkali metal cations to polyethers have been reached in these ranges. Therefore, the limiting dissociation energies can then be correlated to the corresponding

slope values. Thus, the data in Table 1 also show that the dissociation energies decrease in the order of $Na^+ > K^+ > Cs^+$ for each polyether and an order of PEG ≈ PPG > PTHF is obtained for each cation.

The finding that the dissociation energies decrease with the increasing cation size is entirely consistent with those obtained by Armentrout and coworkers for dimethyl ether and dimethoxy ethane using guided ion beam mass spectrometry [90, 91] and with other works [87, 88] as well as the results of a theoretical work from our group [96]. This order for polyether complexation with an alkali metal ion otherwise can be expected on the basis of a simple consideration by taking into account that due to the electrostatic interactions between the ligand and the metal ion, the larger the cation size is the longer the metal-ligand distance, i.e., the lower the bond dissociation energies. On the other hand, the corresponding slopes, hence the bond dissociation energies for PEG and PPG, appear to be quite similar; however, the slopes for PTHF are markedly lower. This finding can also be rationalized respecting the longer O–O distances in PTHF as compared to those in PEG and PPG. PEG and PPG contain C–C–O units and PTHF is composed of –C–C–C–C–O- moieties (see Scheme 1); therefore, within a certain metal–ligand distance more PEG and PPG units containing more oxygen atoms can be wrapped around a metal ion and/or to attain a given coordination number. Thus, oxygen atoms in PTHF must locate farther from the metal ion due to the increased space required by the longer PTHF units reducing the bond strength between the oxygen atoms and the metal ion as opposed to PEG and PPG.

5. 2. Estimation of activation energy from the survival yields: fragmentation study of leucine enkephalin and polyethers by tandem mass spectrometry

SY curves play a significant role in characterizing the energetics of fragmentations in CID. In addition, the kinetic feature of the fragmentations can also be found. SY curve is mainly dependent on the time scale of the mass spectrometric experiments which depends on the instrument time-window [47-49]. Two combined factors determine the SY versus collision energy curve, the first one is the corresponding internal energy-dependent unimolecular dissociation rate constant and the second one is the time passed for fragmentation. In most of the quadrupole-type mass spectrometers such as quadrupole-time-of-flight or triple quadrupole instruments multiple collisions take place in collision cell, so the determination of both the kinetic energy conversion into internal energy and the time elapsed for fragmentation, are not straightforward.

The reasons of these complications are: (1) several collisions of selected ions with the gas molecules that cause stepwise change in the kinetic and internal energy of the precursor ion. (2) As the ion slows down due to the subsequent collisions (kinetic energy loss), the average fragmentation time for an ion with a specific internal energy increases. (3) The collision inelasticity (η), that is the efficiency of conversion of the center-of-mass energy into internal energy, is usually unknown and it is often taken to be 1. (4) Considerable scattering of the selected ion may occur in the collision cell. (5) The processes taking place in a mass spectrometer are stochastic in nature.

Several models including hard-sphere and diffuse-scattering models have been applied based on Monte-Carlo simulations for describing the collisions and the energy transfer, as well as the estimation of the critical energy of fragmentation [97-100]. Masskinetics, a powerful computer program, has been also developed [101]. The collision inelasticity can be set in these

models, however, the selected value of η correlates with the critical energy to be determined (E_0).

To prevail these difficulties related to the multiple collisions and the estimation of E_0 from the SY curves, in this study we will apply two approaches. First we show a simple collision model including formulas for calculating the reaction time, gain of the internal energy and SY data as a function of collision cell length. Secondly, leucine enkephalin was used as a "calibrant" for checking the model validity and to estimate the collision inelasticity [50]. Since the mass spectral properties of the leucine enkephalin are well known, it is often used as a mass spectrometry standard [102]. In addition, assuming the collision inelasticity for compounds with similar degrees of freedom is similar to that for leucine enkephalin. This allows the estimation of the E_0 value from the SY versus collision energy curves.

We selected some polyethers, including PEG, PPG, and PTHF for our studies because of the similar structure in their homologous series. In addition, knowledge of their mass spectrometric behavior is important for the characterization of these polyethers.

Basic relationships used for the derivation of the collision model for the multiple collisions

Internal energy increases and kinetic energy decreases in a single collision. The center-of-mass energy (E_{com}) given by Eq (8) [101]. Denoting $m_g/(m_g+m_p)$ by β Eq (11) comes:

$$E_{com} = \beta E_{kin} \quad (11)$$

As it was shown by Eq (9), ($\Delta E_{int,1}$) is related to E_{com}. In our model, a single value was used for the collision energy-transfer (η), but an extension of the model using Armentrout's energy-transfer distribution defined by Eq (21) in [103] was also made for comparison. Survival yield (SY) results of our estimation using a single η value are in good agreement with those of the model extended with the η distribution, which may support the validity of our model.

The kinetic energy loss of an ion with a mass of m_p in a single collision can be given by Eq (12) [101].

$$\Delta E_{kin} = -E_{com} \frac{2m_p[1-\cos\theta(1-\eta)]+\eta m_g}{m_p+m_g} \quad (12)$$

where θ is the scattering angle.

Assuming random scattering angles, and averaging over all the possible scattering angles Eq (12) reduces to Eq (13) [101].

$$\Delta E_{kin} = -E_{com} \frac{2m_p+\eta m_g}{m_p+m_g} \quad (13)$$

Denoting $\frac{2m_p+\eta m_g}{m_p+m_g}$ by γ the kinetic energy loss of the precursor ion in a single collision can be given by Eq (14).

$$\Delta E_{kin} = -\gamma E_{com} \quad (14)$$

Time elapsed between two subsequent collisions

The mean free path (λ) (i.e., the distance between two subsequent collisions) can be expressed as:

$$\lambda = \frac{k_B T_g}{\sigma_P P_g} \quad (15)$$

where σ_P is the collision cross-section of the ion (assuming that its cross-section is much larger than that of the collision gas), k_B is the Boltzmann constant, Pg and Tg is the pressure and the temperature of the collision gas, respectively.

The average collision number ($\bar{Z}$) of the precursor ions traveling through the collision cell of length L can be expressed by Eq (16):

$$\bar{Z} = L/\lambda \quad (16)$$

The velocity (v) for the precursor ion with mass, m and kinetic energy E_{kin} is:

$$V = \sqrt{\frac{2E_{kin}}{m}} \quad (17)$$

and the time elapsed between two subsequent collisions (τ) is given by:

$$\tau = \lambda \sqrt{\frac{m}{2E_{kin}}} \quad (18)$$

Internal energy increase and kinetic energy loss in multiple collisions

In the quadrupole-type mass spectrometers several collisions may occur at the operating pressure of the collision cell, therefore, in each collision the kinetic energy decreases by a value of $-\gamma E_{com}$. Thus, the kinetic energy after the first collision will be (by combining Eq (11) and Eq (14)):

$$E_{kin,1} = E_{kin,0} - \beta\gamma E_{kin,0} = E_{kin,0}(1 - \beta\gamma) \quad (19)$$

where $E_{kin,o}$ is the initial kinetic energy of the precursor ion.

The kinetic energy of the precursor ion after the i^{th} collision can then be expressed by Eq (20):

$$E_{kin,i} = E_{kin,0}(1 - \beta\gamma)^{i} \quad (20)$$

By combining Equations (11), (9) and (20) the increase in the internal energies after the first and the i^{th} collision is given by Eq (21) and Eq (22), respectively.

$$\Delta E_{int,1} = \eta\beta E_{kin,0} \quad (21)$$

$$\Delta E_{int,i} = \eta\beta E_{kin,0}(1 - \beta\gamma)^{i-1} \quad (22)$$

Therefore, the total increase in internal energy ($E_{int,inc}$) of the precursor ion gained through collisions can be calculated as the sum of a geometric sequence that can be given by Eq

(23) (Providing that the kinetic energy of the ion remained after the last collision is higher than the thermal energy of the surrounding gas).

$$E_{int,inc} = \sum_{i=1}^{z} \Delta E_{int,i} = \frac{\eta E_{kin,0}}{\gamma}[1-(1-\beta\gamma)^z] \quad (23)$$

The internal energy of the precursor ion (E_{int}) is then expressed by Eq (24):

$$E_{int} = E_{int,0} + \frac{\eta E_{kin,0}}{\gamma}[1-(1-\beta\gamma)^z] \quad (24)$$

where $E_{int,o}$ is the initial internal energy of the precursor ion.

Estimation of the survival yield at the exit of the collision cell

Due to the collisions the kinetic energy of the ion will decrease according to Eq (20), thus the velocity and the time (τ_i) between the i^{th} and $i+1^{th}$ can be expressed by Eq (25) and Eq (26), respectively.

$$v_i = \sqrt{\frac{2E_{kin,0}(1-\beta\gamma)^i}{m}} \quad (25)$$

$$\tau_i = \lambda\sqrt{\frac{m}{2E_{kin,0}(1-\beta\gamma)^i}} \quad (26)$$

The total transit time is the sum of the time elapsed between the subsequent collisions, i.e.,

$$\tau = \sum_{i=0}^{z-1} \tau_i = \lambda\sqrt{\frac{m}{2E_{kin,0}}}\left(1+\frac{1}{\sqrt{1-\beta\gamma}}+\cdots+\frac{1}{\left(\sqrt{1-\beta\gamma}\right)^{z-1}}\right) \quad (27)$$

where Z is the total number of collisions. Interestingly, the total transit time through the quadrupole can be calculated as the sum of a geometric sequence of Eq (27), i.e.,

$$\tau = \lambda\sqrt{\frac{m}{2E_{kin,0}}}\left[\frac{1-(1-\beta\gamma)^{-z/2}}{1-(1-\beta\gamma)^{-1/2}}\right] \quad (28)$$

The error of our estimation was evaluated by comparing our results to the simulations of Lock et al., which were based on the ion optics software SIMION [104].

Our model was utilized for calculating the transit time and the exit energy of the ions with the same parameters as Lock et al. used for their simulations: 15.2 cm collision cell filled with 1 mTorr of argon, m/z = 609 with a collisional cross-section of 2.6×10^{-18} m^2 and with an initial energy of 30 eV. A good agreement was found between the results obtained by our model and the SIMION simulation. The average transit time was 80 μs by SIMION and 74 μs calculated with Eq (28), the average exit energy of the ions was 5.5 eV by SIMION and 5.9 eV calculated with Eq (20) Lock et al. determined the variation in exit energy of the ions with the collision cell pressure. As Fig. 11 shows, our estimation (Eq. 20) is in good agreement with the results of the SIMION simulation.

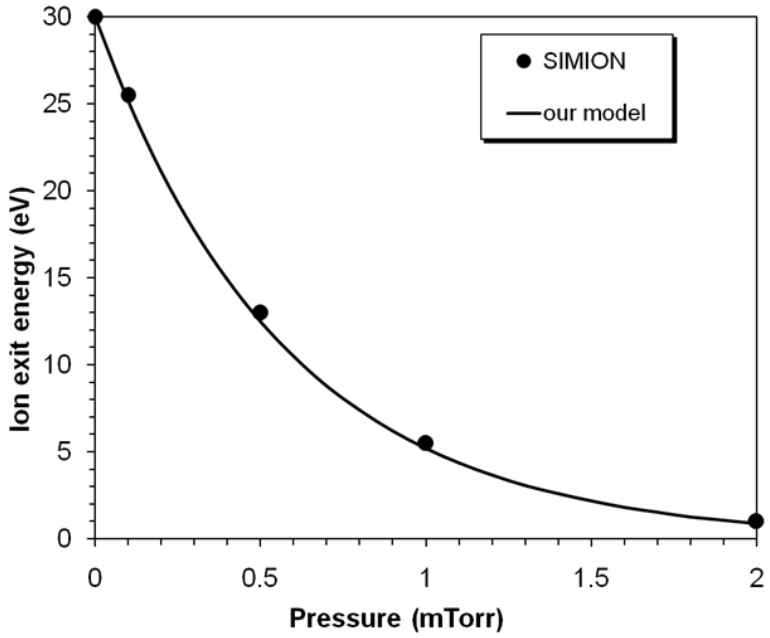

Fig. 11. Variation in ion exit energy with the collision cell pressure determined with SIMION simulations by Lock *et al.* [104] (circles) and by our model (line). Calculation parameters: 15.2 cm collision cell filled with argon, *m/z* = 609 with a collisional cross-section of 2.8×10^{-18} m^2 and with an initial energy of 30 eV.

To calculate the survival yield (SY) the internal energy-dependent rate constant $k(E_{int})$ and the time for fragmentation should be considered. In each collision the internal energy of the precursor ion will increase according to Eq (22). After the i^{th} collision the precursor ion will have $E_{int,i}$ internal energy corresponding to a rate constant $k(E_{int,i})$. Let the time for the fragmentation with a rate constant $k(E_{int,i})$ τ_i (time elapsed between i^{th} and $i+1^{th}$ collision) then the fraction of the undecomposed precursor ion (SY_i) for this collision will be:

$$SY_i = \exp\left[-k\left(E_{int,i}\right)\tau_i\right] \quad (29)$$

The survival yield (SY(L)) at the exit of the collision cell, i.e., at length L is therefore the product of SY_i that can be given by Eq (30).

$$SY(L) = \exp[-\sum_{i=0}^{Z-1} k(E_{int,i})\tau_i - k(E_{int,Z})\tau_r] \quad (30)$$

where Z is the integer part of $\bar{Z}$, i.e., the total number of collisions and τ_r is the remaining time for the ion after the last collision (Z) to reach the exit of the collision cell (will be discussed below).

The $E_{int,i}$ and τ_i can then be calculated by Eq (24) and Eq (26), respectively. After the last collision (Z) the ion will travel a distance of $(\bar{Z} - Z)\lambda$ on the average to the exit of the collision cell and the time required for traveling through this distance comes as Eq (31).

$$\tau_r = \left(\bar{Z} - Z\right)\lambda / v_r \quad (31)$$

where v_r is the velocity of the ion after the last collision.

Testing the model using leucine enkephalin

Using the collision model and RRKM algorithm to fit the experimental survival yield (SY) versus collision energy curve

Using Eq (30), (24) and (26), the SY values can be calculated at the exit of the collision cell (at length L), which is finally observed in the MS experiment. The energy-dependent rate constant $k(E_{int})$ for leucine enkephalin was calculated using the RRKM approximation [105] (Eq. 7) for each collision.

$$k(E_{int}) = \frac{\sigma W^{\#}(E_{int} - E_0)}{h\rho(E_{int})}$$

In the RRKM algorithm the suggested values of E_o, (1.05 eV), as well as the reactant and transition state frequencies for the protonated leucine enkephalin were used [102]. The initial internal energy of protonated leucine enkephalin was estimated with Eq (32) [106].

$$E_{int,0} = c(v,T)sk_BT \quad (32)$$

where s and T are the degrees of freedom and the temperature, respectively, k_B is the Boltzmann's constant and c(ν,T) is the fraction of the active oscillators which is 0.225 at the source temperature of our ESI experimental conditions. The fraction of the active oscillators was calculated based on the Eq (9) in [106], the state frequencies were obtained from [102].

The algorithms of the collision model and the RRKM model were implemented into the spreadsheet software. The only unknown parameter in the collision model is the collision inelasticity (η) (i.e., the fraction of center-of-mass energy transferred to internal energy in a single collision). The SY values of leucine enkephalin calculated at the exit of the collision cell of the Q-TOF and TQ instruments were fitted to the experimental SY versus collision energy curve using the spreadsheet software by varying the value of η until the best fit was obtained.

The SY values as a function of the collision energy obtained by the Q-TOF and TQ instruments together with the fitted curve using the RRKM-approximation are plotted in Fig. 12.

Fig. 12 shows a good agreement between the experimental and the fitted curves. In the case of the Q-TOF instrument η = 0.43 while in the TQ experiment higher values of η were obtained, i.e., 0.53 (at 1 mTorr), 0.57 (at 0.7 mTorr) and 0.58 (at 0.5 mTorr). These higher values may be attributed to the fact that a more effective energy transfer takes place with Ar than with N_2 molecules. (Note that N_2 collision gas was applied in the Q-TOF and Ar in the TQ instrument). Furthermore, experiments were done with Ar collision gas on the Q-TOF instrument, and η = 0.55 was obtained, which is in good agreement with the η values of the TQ

instrument. On the other hand, the η values obtained at different Ar pressures in the collision cell show reasonably well agreement, supporting that the simplified collision model is capable of the description of multiple collisions and predicting the SY values as a function of the collision energy.

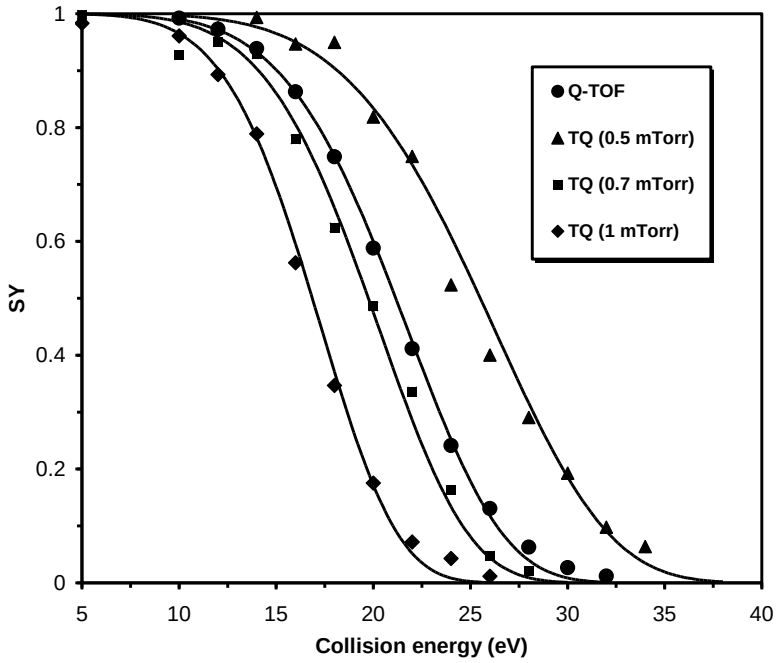

Fig. 12. The SY values for leucine enkephalin as a function of the collision energy measured by quadrupole-time-of-flight (Q-TOF) and triple quadrupole (TQ) instruments. Parameters for Q-TOF: collision gas: N_2, collision cell length: 0.08 m, collision cell pressure: 0.8 Pa. Parameters for TQ: collision gas: Ar, collision cell length: 0.25 m, collision cell pressure: 0.132 Pa (1 mTorr), 0.092 Pa (0.7 mTorr) and 0.066 Pa (0.5 mTorr). The other parameters are the same for both instruments. The solid lines represent the calculated curves using the following parameters: $E_{int,o}$ = 2 eV, T_{coll} = 293 K, $\sigma = 1.62\times10^{-18}$ m^2, E_o = 1.05 eV. The η values providing the best fit for the Q-TOF, TQ at 1 mTorr, 0.7 mTorr and 0.5 mTorr were found to be 0.43, 0.53, 0.57 and 0.58 respectively.

Our model was extended by taking into account the initial internal energy distribution, which was calculated based on Eq (15) in [106]. The SY values at the end of the collision cell were calculated at different initial internal energies corresponding to the width of the distribution, and weighted by the distribution function (see Fig. 13). The results of the original estimation are in good agreement with the results of the extended model.

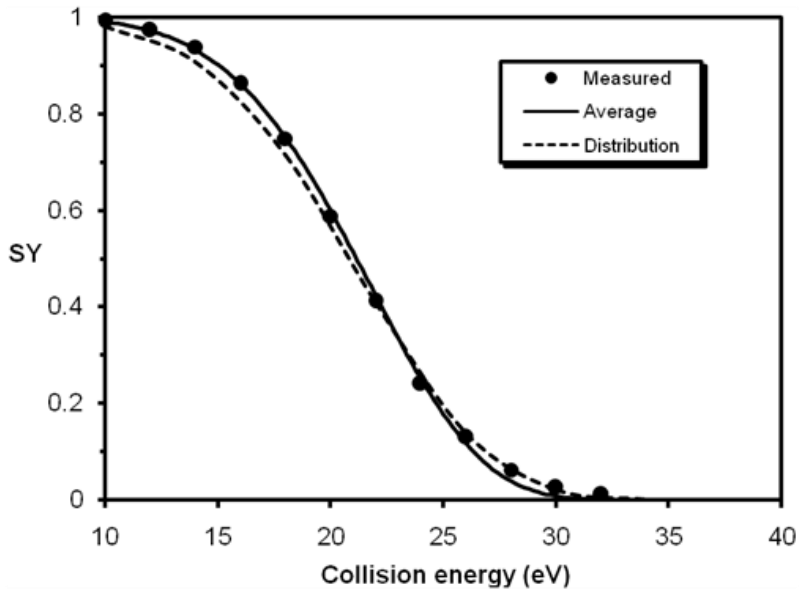

Fig. 13. The SY values for leucine enkephalin as a function of the collision energy measured by the quadrupole-time-of-flight (Q-TOF) instrument. Parameters for Q-TOF: collision gas: N_2, collision cell length: 0.08 m, collision cell pressure: 0.8 Pa. The solid line represents the calculated curve using the average initial internal energy of 2 eV, the dashed line is the curve using initial internal energy distribution. Calculation parameters: T_{coll} = 293 K, $\sigma = 1.62\times10^{-18}$ m^2, E_o = 1.05 eV, η = 0.43. The RRKM model was used for the calculation of the rate constants.

Using the collision model and RRK algorithm to fit the experimental survival yield (SY) versus collision energy curve

The experimental SY curve for leucine enkephalin was also approximated by the RRK model (Eq. 6).

$$k(E_{int}) = A(1 - \frac{E_0}{E_{int}})^{s_{eff}}$$

where S_{eff} is the number of effective oscillators.

In Fig. 14 the SY versus collision energy curve determined by the Q-TOF instrument together with the fitted curves calculated by RRKM and RRK model are shown for comparison.

Fig. 14 indicates a good agreement between the experimental and the fitted curve using the RRK model. In this fitting E_o was set to 1.05 eV and η = 0.43 was used in the calculations, while A and S_{eff} were varied until the best fit to the experimental SY values was obtained. The fit (Fig. 14 Gray line) is good and the rate constants calculated by the RRKM and RRK also agree well (Fig.14 inset). The value of S_{eff} is also reasonable since in the RRK model the total number of oscillators (s = 228) is reduced to about one fifth. (The total number of oscillators, e.g. the total degrees of freedom (DOF) is defined as 3×N–6, where N is the number of the atoms in the precursor ion). The value of A of RRK (8×10^7) is considerably lower than that can be calculated from RRKM (6×10^{10}).

The reason for the large difference in the A values obtained by the two methods in spite of the fact that the $k(E_{int})$ values agree well, is that the RRK does not take into account the variation of S_{eff} with the internal energy. Moreover, despite the simplicity and some drawbacks of the RRK model discussed above it may be still capable of estimation of the critical energies especially of compounds with similar degrees of freedom.

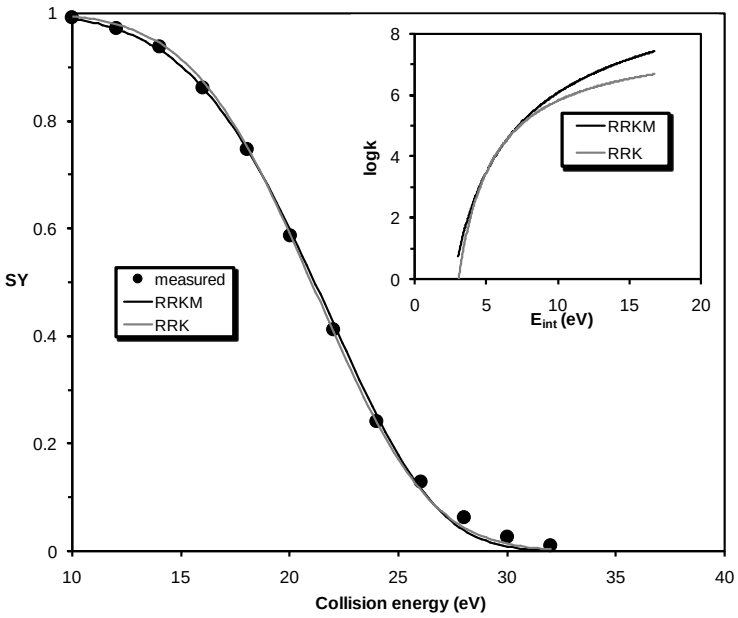

Fig. 14. The SY values for leucine enkephalin as a function of the collision energy measured by the quadrupole-time-of-flight (Q-TOF) instrument. Parameters for Q-TOF: collision gas: N_2, collision cell length: 0.08 m, collision cell pressure: 0.8 Pa. The solid line represents the calculated curve using the RRKM model. The dashed line is the fitted curve using the RRK model, fitted parameters for RRK are $A = 8\times10^7$ and $S_{eff} = 43$. The other calculation parameters are the same as in Fig. 12 caption.

Estimating the efficiency of the kinetic to internal energy conversion for leucine enkephalin in quadrupole-time-of-flight instrument

Using Eq (30) the SY values can be calculated as a function of the distance from the entrance of the collision cell. The variations of the kinetic and internal energy, as well as the survival yield through the collision cell of our Q-TOF instrument for the leucine enkephalin calculated by the model and the RRKM algorithm are presented in Fig. 15.

As it can be seen in Fig. 15. using the parameter $\eta = 0.43$ the internal energy increases from the initial 2 eV (Eq. 32) up to 7.1 eV while the initial kinetic energy of 24 eV decreases to 1.3 eV due to the subsequent collisions. In this example about 20 % of the Lab frame kinetic

energy is converted into internal energy of the precursor ion. Interestingly, Eq (23) also shows that in the case of η = 1 and $m_p >> m_g$ and at sufficiently large number of collisions maximum half of the initial kinetic energy can be converted into internal energy (in that case $(1 - \beta\gamma) \approx 0$ and $\gamma \approx 2$).

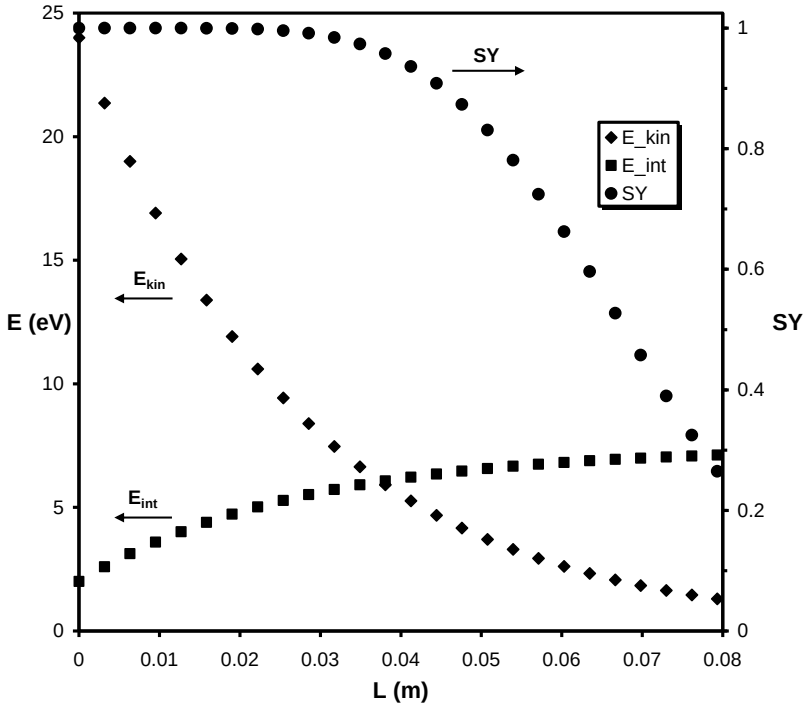

Fig. 15. Variations of the kinetic and internal energy, as well as the survival yield for the leucine enkephalin as a function of the distance from the entrance of the collision cell. L = 0.08 m corresponds to the exit of the collision cell. Parameters are: $E_{kin,o}$= 24 eV, $E_{int,o}$= 2 eV, p_{coll} = 0.8 Pa, T_{coll} = 293 K, cross section = 1.62×10^{-18} m^2, η = 0.43, E_o = 1.05 eV.

It is also evident from Fig. 15. that the dissociation of the precursor ion mainly take places in the second half of the collision cell, in good agreement with the results obtained using similar kinematics with Monte-Carlo simulations [97, 100].

Estimating the E_o values for the polyethers

Our next aim was to estimate the critical energies of the polyethers such as (PEG), (PPG) and (PTHF). The calculation of $k(E_{int})$ by the RRKM model for polyethers should involve the reactant and transition state frequencies which are not known for this class of polymers. One possible way to overcome these issues for estimation of E_o is to apply RRK model.

However, involving the size-effect, i.e., the DOF effect into the RRK model is not straightforward. Therefore, to avoid a DOF effect on the SY curves of these polyethers with similar degrees of freedom to that of leucine enkephalin were investigated as a function of collision energies. The SY curves as a function of collision energy for the lithiated polyethers and leucine enkephalin are plotted in Fig. 16.

As seen in Fig. 16. the SY curves for each polyether shifted to higher collision energies, indicating that the lithiated polyethers with similar degrees of freedom to that of leucine enkephalin required higher collision energy for fragmentation. This also suggests that the critical energies for fragmentation of the lithiated polyethers are higher than that of leucine enkephalin. On the other hand, it is also seen in Fig. 16. that all polyethers require similar collision energy for fragmentation. This observation also implies that the critical energies for fragmentation of these polyethers are very similar.

To estimate the E_o values of these polyethers the RRK model was applied. In these calculations the numbers of effective oscillators, as well as the energy transfer efficiency η = 0.43 were kept constant as obtained for leucine enkephalin. Although η and S_{eff} were taken arbitrarily to be the same for leucine enkephalin and polyethers with similar degrees of freedom, there are some indications and thorough theoretical investigations which may support the close validity of these approximations. For example, it has been demonstrated that the values $c(\nu,T)$ as

a function of the internal energy vary similarly for compounds of higher molecular weight [106]. While keeping η and S_{eff} values constant the values of A and E_o were varied to obtain the best fit to the experimental SY curves. The results of these calculations are summarized in Table 2. The fitted SY curves are shown by solid lines in Fig. 16.

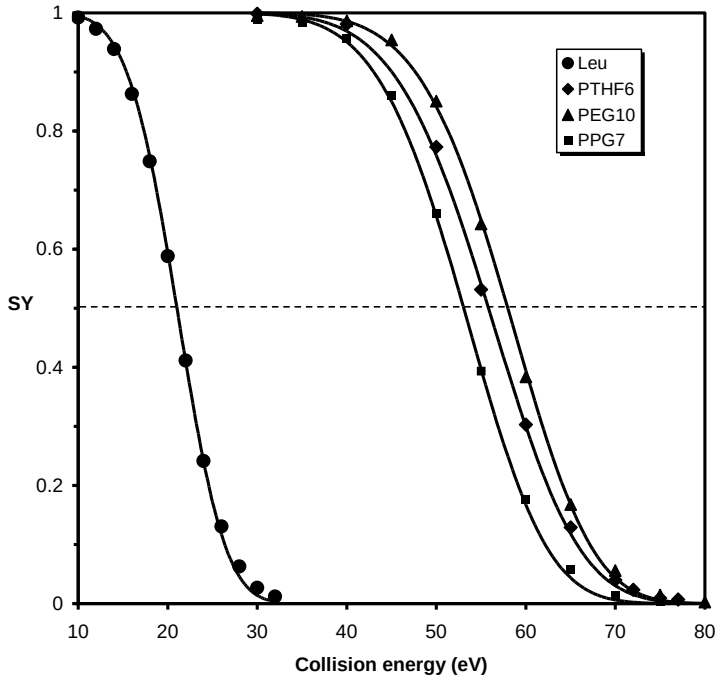

Fig. 16. The SY versus collision energy curves for the PTHF6, PEG10 and PPG7 determined by Q-TOF. The SY versus collision energy for leucine enkephalin is also presented for comparison. The solid lines represent the fitted curves by the RRK model. The parameters used for the fitting are $E_{int,o}$ = 2 eV, p_{coll} = 0.8 Pa, T_{coll} = 293 K, $\sigma = 1.5\times10^{-18}$ m^2 and η = 0.43. The estimated values of A and E_o for PTHF6, PEG10 and PPG7 are given in Table 2. Cross-sections (σ) for the polyethers were determined from the work of Bowers et al. [107].

As it turns out from the data of Table 2, the E_o values for each polyethers are significantly higher than for leucine enkephalin it is in good agreement with the expectation based on the SY curves. It is also evident from Table 2, that the E_o values for polyethers are

close together, although PEG10 shows a little bit higher critical energy for fragmentation as compared to the other two polyethers.

	Leu	**PTHF6**	**PEG10**	**PPG7**
DOF	228	240	216	216
S_{eff}	43	43	43	43
A	$8x10^7$	$2.5x10^8$	$5.5x10^8$	$3x10^8$
E_o (eV)	1.05	2.46	2.72	2.45

Table 2. The DOF and S_{eff} values used and the values of A and E_o estimated from the RRK fitting for the PTHF6, PEG10 and PPG7. For comparison, these values are also shown for leucine enkephalin. The numbers in the polyethers's names stand for the number of repeat units.

The estimated A values for the polyethers are somewhat higher than for leucine enkephalin. Moreover, the estimates of the A values within the group of the studied polyethers are also very similar - in good agreement with the expectation based on the structural similarities between these polyethers.

The critical energy obtained for the lithiated PEG10 is very close to that obtained by high-level quantum chemical calculations for PEG6 (2.3 eV and 2.8 eV at the levels of theory B3LYP and M05-2X, respectively for the main fragmentation pathway) [108]. It should be noted, however, that according to the theoretical calculations performed on lithiated PEG with a number of repeat units n (from n = 2 up to n = 6) the critical energy for fragmentation showed a chain-length dependence with a decrease of barrier height from 2.7 eV (n = 2) to 2.3 eV (n = 6) at B3LYP and from 3.0 eV (n = 2) to 2.8 eV (n = 6) at M05-2X.

Although there are no calculations for PEG with higher polymerization degrees it seems likely that at around n = 6 the critical energy levels off, thus ca. 2.3 eV at B3LYP and 2.8 eV at M05-2X can also be expected for PEG10. Unfortunately, no such calculations are available for PTHF and PPG. Nevertheless, the relatively good agreement between the theoretical and the estimated values of E_o for PEG may validate the correctness of our approximations used for the estimation of the E_o values of polyethers.

5. 3. Electrospray ionization tandem mass spectrometry of the star-shape propoxylated diethylenetriamine polyols

A study about the arm length distribution of the four-arm star propoxylated ethylenediamine polyol determined by tandem mass spectrometry was reported by our research group [109]. The CID of the four-arm polyol-produced product ions are formed by the loss of the whole oligomeric arm and no backbone fragmentation was observed. We were able to explore the initiation and chain length propagation properties of this polyol by MS/MS. It was expected that there is no backbone fragmentation in the case of propoxylated DETA polyols product ions also. However, there are considerable differences between the ethylenediamine and DETA-based polyols: (1) DETA contains two primary and one secondary amines (four arms linked to primary amines and one to the secondary amine), which may affect the initiation and chain length propagation, (2) more fragmentation pathway can be expected in the case of propoxylated DETA polyols because of its more complex structure. These differences defend our goal to explore the fragmentation mechanism of the five arm star propoxylated DETA polyol and determine the distribution of the propylene oxide units within the oligomer.

Fig. 17 shows the ESI-MS spectrum of an industrial propoxylated diethylenetriamine (Petol PA 500-5D) with an approximate number average molecular weight of 500 g/mol. Two series can be observed corresponding to the protonated and sodiated propoxylated DETA polyol.

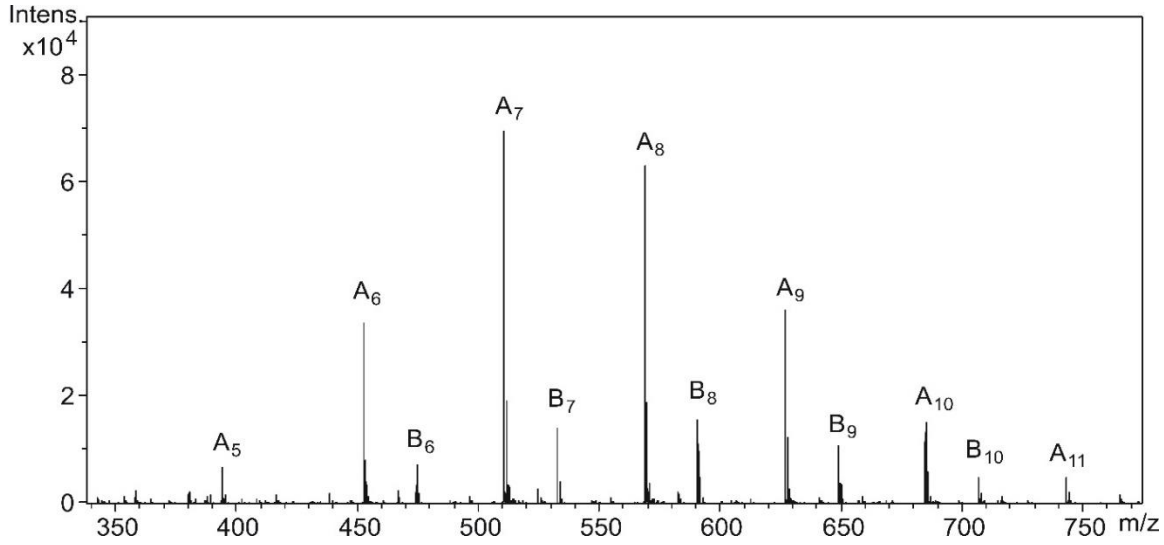

Fig. 17. ESI MS spectrum of the propoxylated diethylenetriamine. The A and B series represent the protonated ($[M+H]^+$) and sodiated ($[M+Na]^+$) adduct ions, respectively. The numbers in the indexes refer to the number of propylene oxide units.

As indicated in Fig. 17, oligomers with five to eleven repeating units appeared in the mass spectrum. The repeating units can be distributed within the oligomers in many different ways (e.g. with the notation of Scheme 1, in the case of 7 repeating units two examples are the following: a = 1, b = 2, c = 2, d = 1, e = 1 and a = 2, b = 2, c = 1, d = 1, e = 1).

Tandem mass spectrometric experiments were performed in order to explore the structurally important product ions of the propoxylated DETA polyols and to gather information about the length of the "PPG arms". The MS/MS spectra of the sodiated propoxylated DETA polyol did not inform us about the arm length distribution, because fragmentation of the

backbone was observed. But the polyether chains remained intact under the collision-induced dissociation of the protonated propoxylated DETA polyol, making possible the deduction of the chain-length distribution. As a representative example, Fig. 18a shows the product ion spectrum of the protonated propoxylated DETA polyol containing 10 repeating units.

As seen in Fig. 18a, two product ion series are produced by C-N cleavage in the DETA moiety of the protonated polyol. Probably, immonium cations were formed. Scheme 2 shows the proposed mechanism for fragmentation of the protonated propoxylated DETA. The charge is located at the initiator moiety on one of the nitrogen atoms inducing the formation of two different product ion series as shown in Scheme 2. The series m/z 160, 218, 276, 334, 392, 450 correspond to the product ions with two arms, and a + b equals 2, 3, 4, 5, 6, or 7, respectively (see Scheme 2a). The other series at m/z 261, 319, 377, 435, 493, 551 correspond to the product ions with three arms, and a + b + c equals 3, 4, 5, 6, 7 or 8 respectively (see Scheme 2b). No product ions were recorded with a + b less than 2 or more than 7, and a + b + c less than 3 or more than 8. It suggests, that the rate of the initiation is greater than that of the chain propagation.

It is even more evident, that the propagation of the PPG arms starts after the first five propylene oxide units were attached to the five initiation sites, on the basis of the MS/MS spectrum of the protonated propoxylated DETA polyol containing five repeating units (shown in Fig. 19a). As seen in Fig. 19a, only two product ions were observed, which indicates, that all the five arms contain exactly one repeating unit (the product ion at m/z 160 has two arms with a = b = 1, and the ion at m/z 261 has three arms with a = b = c = 1).

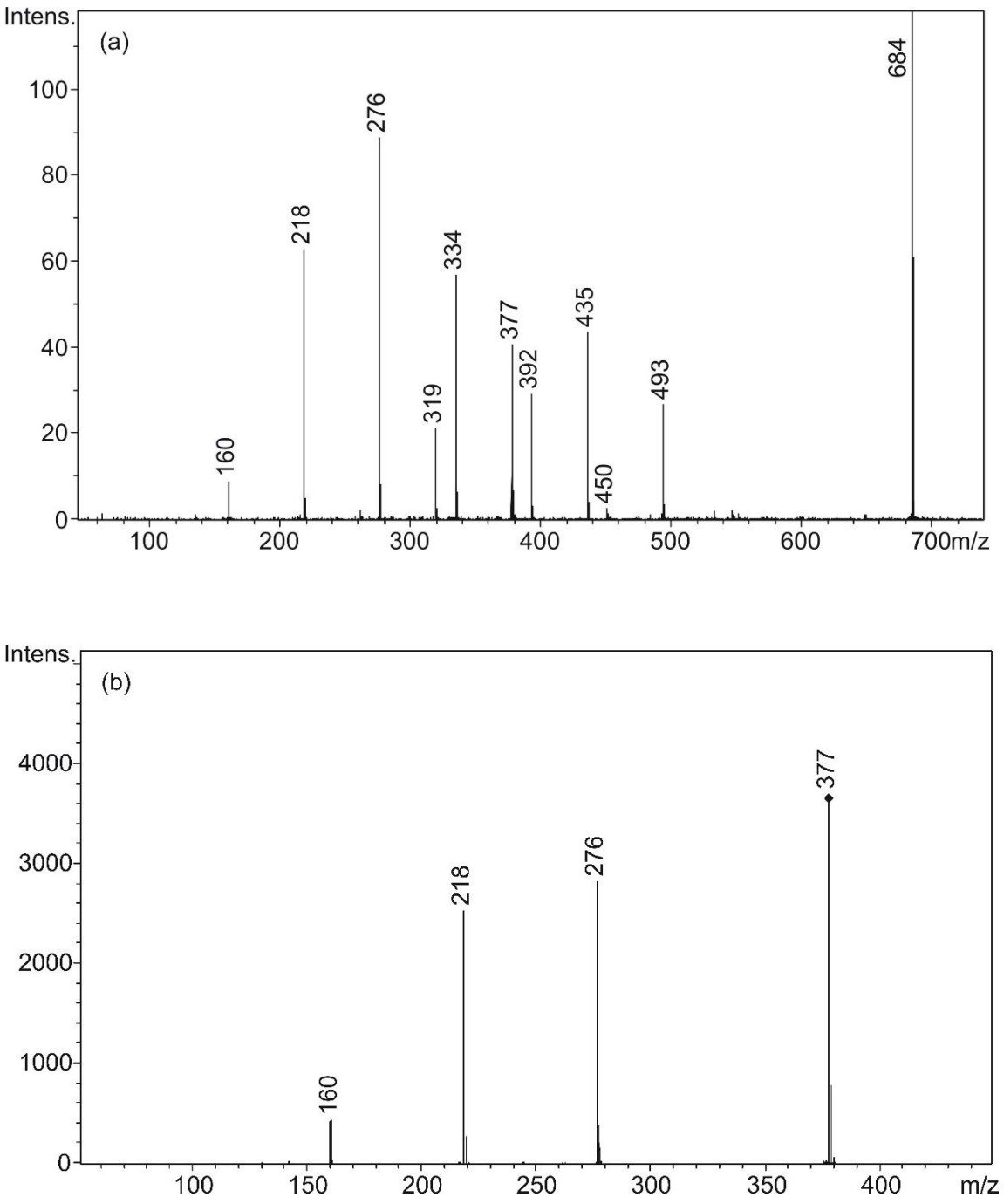

Fig. 18. (**a**) ESI-MS/MS spectrum of protonated propoxylated diethylenetriamine with a number of propylene oxide units n = 10 recorded at a laboratory frame collision energy of 32 eV. (**b**) Pseudo ESI-MS^3 spectrum of the three arm product ion with 5 repeating units (*m/z* 377) recorded at a laboratory frame collision energy of 17 eV. The precursor ion was generated by in-source collision-induced dissociation.

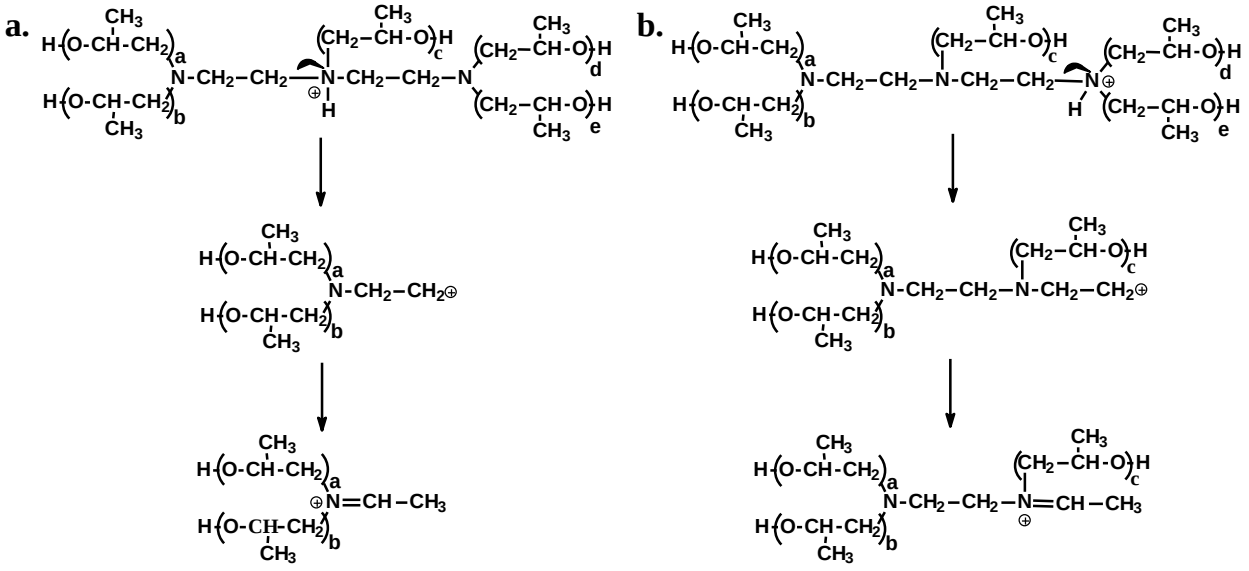

Scheme. 2. Proposed mechanism for fragmentation for the protonated propoxylated diethylenetriamine.

Furthermore, MS^3 experiments also confirm that the initiation is faster than the chain propagation. As Fig. 18b shows, no product ions were generated with a or b equals zero or a + b = 5 (see Scheme 1) in the consecutive fragmentation of the three arm product ion with 5 repeating units (m/z 377). Moreover, if the three arm product ion with 3 repeating units (m/z 261) was selected as the precursor ion in the MS^3 experiment, only one product ion appeared in the MS^3 spectrum at m/z 160 with a = b = 1 (shown in Fig. 19b).

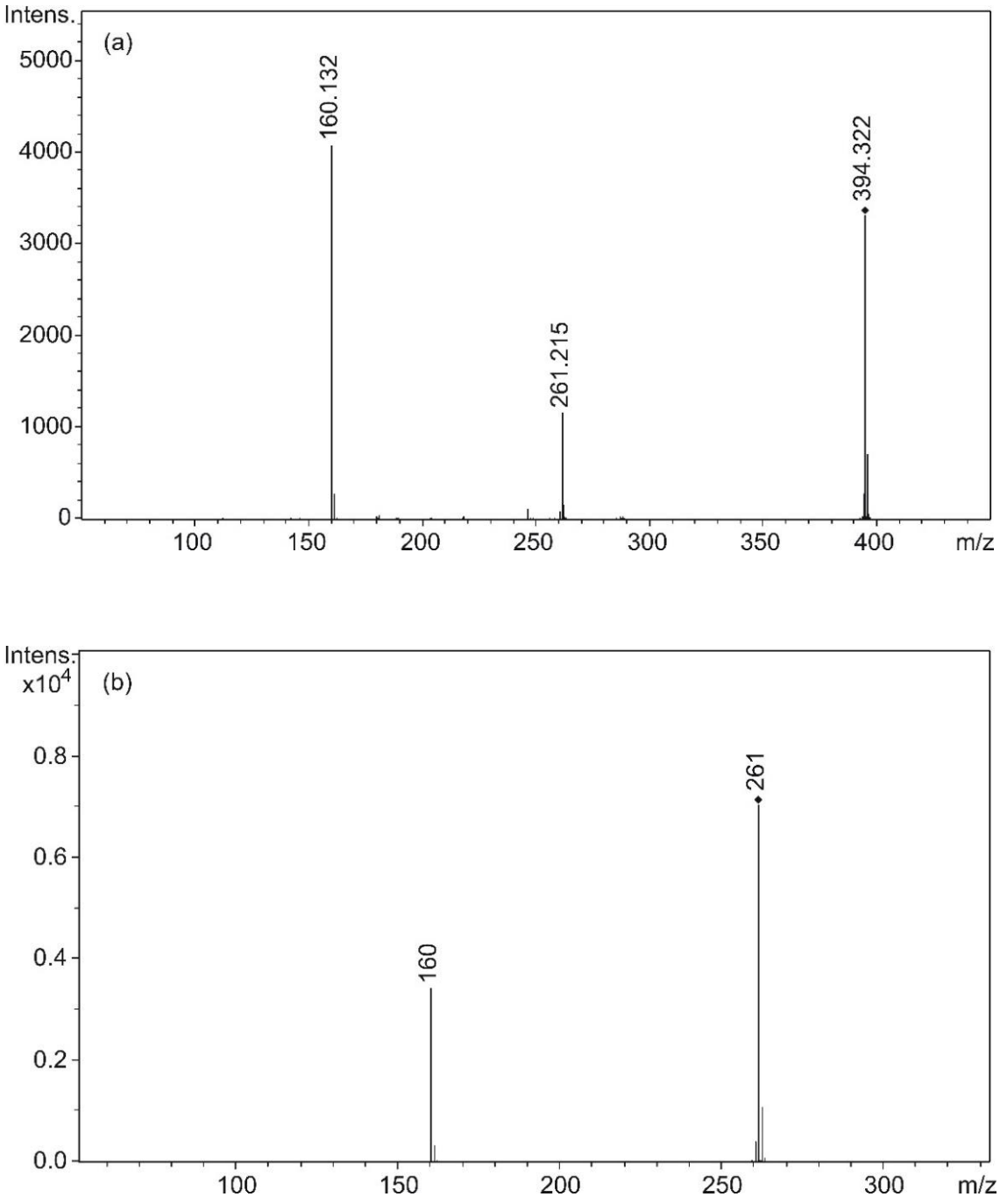

Fig. 19. (**a**) ESI-MS/MS spectrum of protonated propoxylated diethylenetriamine with a number of propylene oxide units n = 5 recorded at a laboratory frame collision energy of 21 eV. (**b**) Pseudo ESI-MS^3 spectrum of the three arm product ion with 3 repeating units (*m/z* 261) recorded at a laboratory frame collision energy of 8 eV. The precursor ion was generated by in-source collision-induced dissociation.

In further studies, the chain propagation mechanism of the polymerization reaction was investigated by comparing the experimentally determined chain-length distribution within the oligomer to the calculated one. MS/MS measurements can provide information about the arm-length distribution, as it was shown for the four arm star propoxylated ethylenediamine polyols [109]. Although in the propoxylated DETA four arms are linked to primary amines and one to the secondary amine, we presumed that the repeating units are randomly distributed in the oligomer and attach to the initiation sites with the same probability. Considering the fragmentation path which results the product ions with two arms, we can arrange the repeating units on the two sides of the initiator (a, b, and c, d, e, Scheme 2a) according to a binomial distribution (Eq. 33).

$$f(m = k + 2) = \binom{n-5}{k} p^k (1-p)^{(n-5)-k} = \binom{n-5}{k} 0.4^k 0.6^{(n-5)-k} \quad (33)$$

where f(m) is the probability of finding m repeat units on the arms of one of the primary amine of the initiator (a + b = m), n is the total number of repeat units, p is the probability of attaching one repeat unit on the arms of a primary amine of the initiator. The theoretical distribution takes into consideration that only n - 5 units are distributed randomly once the first five propylene oxide units were attached to the five initiation sites. Assuming equal probabilities regarding the addition of a monomer unit to the five arms, it is reasonable to assume that p = 0.4. The distribution of the repeating units between the two sides of the initiator was estimated experimentally on the basis of the intensities of the product ion bearing two arms. Fig 20a and 20b show the calculated Eq (33) and measured intensities of the product ions obtained for the oligomers with the number of propylene oxide units n = 7 and n = 10, respectively, which correspond to n - 5 = 2 and n - 5 = 5 units to be distributed, respectively.

As it turns out from Fig. 20b, there is a good agreement between the theory and experiment, and similar agreement were observed for the oligomers n = 9, 11 or 12. However, if there are only a few repeat units to be distributed among the arms, i.e. 1, 2 or 3 units corresponding n = 6, n = 7 or n = 8, respectively, notable discrepancies were recognized between the experimental and calculated repeat unit distribution, as seen in Fig. 20a for the oligomer n = 7. These discrepancies may be explained by the differences of the fragmentation and/or chain length propagation properties in the case of a very small number of repeat units depending on whether the oligomer has a repeat unit attached to one of the primary or the secondary amine initiation site.

The repeat unit distribution of the other product ion series, namely the fragments having three arms (Scheme 2b), was also compared to the theoretical distribution calculated by Eq (34).

$$f(m = k + 3) = \binom{n-5}{k} q^k (1-q)^{(n-5)-k} = \binom{n-5}{k} 0.6^k 0.4^{(n-5)-k} \qquad (34)$$

where f(m) is the probability of finding m repeat units on the arms of one of the primary plus the secondary amine of the initiator (a + b + c = m), n is the total number of repeat units, q is the probability of attaching one repeat unit on the arms of one of the primary or the secondary amine of the initiator.

Again, supposing that all the growing chain-ends react with the monomer with the same reaction rate, it is reasonable to assume that q = 0.6. Similarly to the previous case (two-arm product ion series) the product ion intensity distributions agree well with those calculated by Eq (34) for the oligomers n = 10 to n = 13. As a representative example, Fig. 20c shows the experimental and calculated repeat unit distribution for the oligomer n = 12. The small deviations between the theoretical and experimental values may be ascribed to a mass-discrimination effect due to mass dependent ion-transmission and/or detection efficiencies.

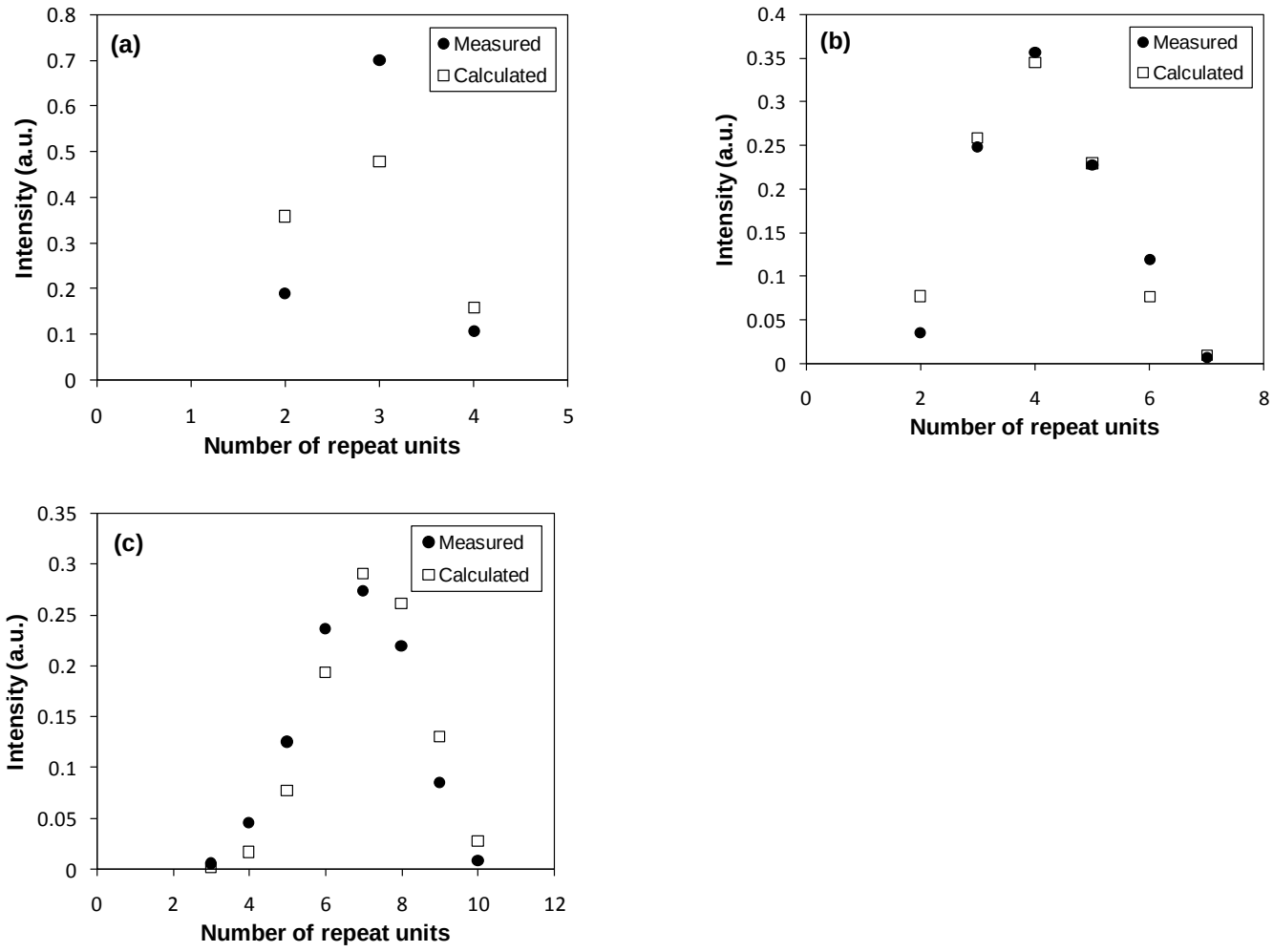

Fig. 20. Measured and calculated ion abundances for two-arm product ions formed from the protonated propoxylated diethylenetriamine with number of propylene oxide units n = 7 (a) and n = 10 (b). The calculated data were obtained using Eq (33). The laboratory frame collision energies for n = 7 and n = 10 were 26 eV and 32 eV, respectively. (c) Measured and calculated ion abundances for three-arm product ions formed from the protonated propoxylated diethylenetriamine with number of propylene oxide units n = 12. The calculated data were obtained using Eq (34). The laboratory frame collision energy was 43 eV.

Another important point of this work is that a linear relationship was found between the collision energy necessary to obtain 50% fragmentation (CE_{50}) and the number of propylene oxide repeat units as shown in Fig. 21.

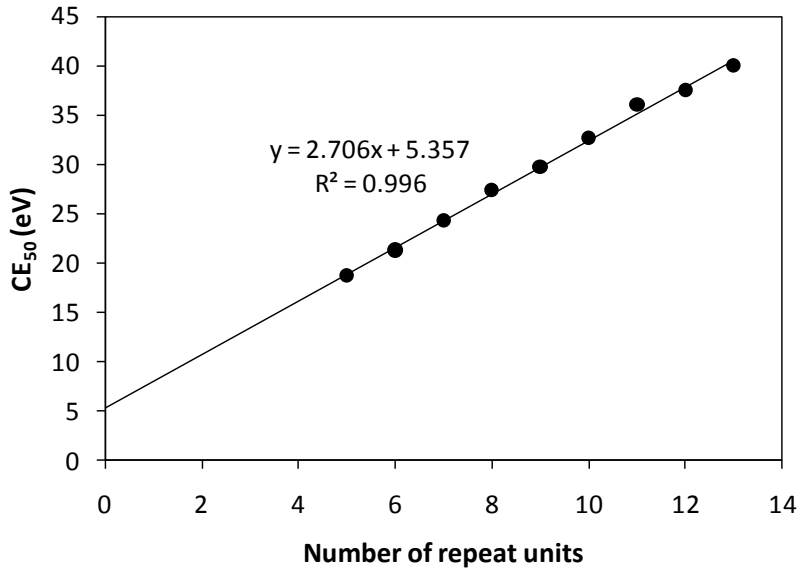

Fig. 21. Variation of the values of CE_{50} with the number of propylene oxide units.

Similar linear relationship between the values of CE_{50} and the mass (or the number of repeat units) has been found for various systems. The practical utility of this relationship is very valuable since it makes possible the automatic gain of the collision energy to obtain structural information such as those presented in this work.

6. SUMMARY

In the first study PEG, PPG and PTHF polyethers were doubly cationized by Na^+, K^+ and Cs^+. Dissociation of these doubly charged polyethers into singly charged polyethers was studied by means of energy-dependent CID tandem mass spectrometry. Results have shown CV_{50} determined for the doubly cationized polyethers of higher degree of polymerization varied linearly with the DOF values. The slopes of the CV_{50} versus DOF curves were correlated with the relative gas-phase dissociation energies for binding of alkali ions to the polyethers. The relative dissociation energies decrease in the order of $Na^+ > K^+ > Cs^+$ for each polyether studied, and an order of PPG ≈ PEG > PTHF could be recognised for each alkali metal ion.

A simple collision model for treating multiple collisions taking place in quadrupole-type mass spectrometers has been developed. It was shown that this model can describe the energetics of the fragmentations. The inelasticity ratio for the leucine enkephalin in quadrupole-time-of-flight and quadrupole instruments was determined by applying of the collision model and RRKM algorithm. If the total degrees of freedom is reduced to about one fifth in RRK formalism, the RRK can give comparable results with those of the more complicated RRKM model. In addition, critical energy (E_0) of lithiated polyethers including PEG, PPG and PTHF with degrees of freedom similar to that of leucine enkephalin can be estimated by this collision model with the RRK formalism. We used polyethers with similar DOF in order to eliminate the effect of DOF on the unimolecular reaction rate constant. Our model which used the RRK formalism, determined that the critical energies needed for fragmentation of studied polyethers were similar. The collision model with the RRK formalism provided critical energy for fragmentation for polyethers comparable to that calculated by high-level quantum chemical calculations reported in the literature.

The collision induced dissociation of the protonated five arm star propoxylated diethylenetriamine polyols was studied under electrospray conditions. The cleavage of the C-N bonds in the initiator moiety results two product ion series. Since no backbone fragmentation of the polyether chains was observed so the initiation and side-chain propagation process of the oligomers could be explored. Considering the chain-length distribution study, the basis of MS/MS spectra has shown it is probable that the rate of the initiation is larger than that of the chain propagation. The propylene oxide repeat units attach to the five arms with approximately the same probability. It should be added that the chain length propagation and/or fragmentation properties can be different in the case of a very small number of repeat units depending on the repeat unit attachment location (one of the primary or the secondary amine initiation site). We also found out that the collision energy necessary to obtain 50% fragmentation (CE_{50}) was linearly dependent on the molecular weight of the polyols.

7. KEYWORDS

collision-induced dissociation

diethylenetriamine

electrospray ionization mass spectrometry

leucine enkephalin

multiple collisions

polyethers

polypropylene glycol

RRK and RRKM model

tandem mass spectrometry

8. REFERENCES

[1] E.d. Hoffmann, V. Stroobant, Mass Spectrometry: Principles and Applications, Wiley & Sons, Baffins Lane, Chichester, West Sussex, PO19 IUD, England, 2002, pp: 5-365.

[2] A.J. Dempster, A new method of positive ray analysis, Physical review D: Particles and fields, 11 (1918) 316-325.

[3] J.H. Gross, Mass Spectrometry, Springer-Verlag, Heidelberg, Germany, 2004, pp:1.

[4] F.P. Guengerich, Thematic minireview series on biological applications of mass spectrometry, The Journal of biological chemistry, 286 (2011) 25417.

[5] S. Banerjee, S. Mazumdar, Electrospray ionization mass spectrometry: a technique to access the information beyond the molecular weight of the analyte, International journal of analytical chemistry, 2012 (2012) 282574.

[6] H.H. Willard, L.L. Merritt Jr, J.A. Dean, F.A. Settle Jr, Instrumental Method of Analysis, 7th ed., Wadsworth Publishing Company, New York, 1988.

[7] G.L. Glish, R.W. Vachet, The basics of mass spectrometry in the twenty-first century, Nature reviews drug discovery, 2 (2003) 140-150.

[8] I.D. Wilson, C. Poole, Handbook of Methods and Instrumentation in Separation Science, Elsevier Ltd, London, 2000, pp: 412–452.

[9] A.P. Bruins, Mechanistic aspects of electrospray ionization, Journal of chromatography. A, 794 (1998) 345-357.

[10] J. Eriksson, D. Fenyo, Mass spectrometry : instrumentation, interpretation, and applications edited by Rolf Ekman [et al], John Wiley & Sons, Inc, Hoboken, New Jersey., 2008, pp: 211.

[11] B.K. Matuszewski, M.L. Constanzer, C.M. Chavez-Eng, Matrix effect in quantitative LC/MS/MS analyses of biological fluids: a method for determination of finasteride in human plasma at picogram per milliliter concentrations, Analytical chemistry, 70 (1998) 882-889.

[12] L. Rachel, G.H. Sleighter, G.H. Patrick, The application of electrospray ionization coupled to ultrahigh resolution mass spectrometry for the molecular characterization of natural organic matter, Journal of mass spectrometry, 42 (2007) 559-574.

[13] S.R. Wilson, Y. Wu, Applications of electrospray ionization mass spectrometry to neutral organic molecules including fullerenes, Journal of the American Society for Mass Spectrometry, 4 (1993) 596-603.

[14] C.E.C.A. Hop, R. Bakhtiar, Electrospray ionization mass spectrometry. Part III: applications in inorganic chemistry and synthetic polymer chemistry, Journal of chemical education, 73 (1996) A162-A169.

[15] M.J. Keith-Roach, A review of recent trends in electrospray ionisation-mass spectrometry for the analysis of metal-organic ligand complexes, Analytica chimica acta, 678 (2010) 140-148.

[16] J.B. Fenn, Electrospray wings for molecular elephants (Nobel lecture), Angewandte Chemie, 42 (2003) 3871-3894.

[17] C.S. Ho, C.W. Lam, M.H. Chan, R.C. Cheung, L.K. Law, L.C. Lit, K.F. Ng, M.W. Suen, H.L. Tai, Electrospray ionisation mass spectrometry: principles and clinical applications, The Clinical biochemist. Reviews / Australian Association of Clinical Biochemists, 24 (2003) 3-12.

[18] P. Kebarle, L. Tang, From ions in solution to ions in the gas phase: the mechanism of electrospray mass spectrometry, Analytical chemistry, 65 (1993) 972A–986A.

[19] J.V. Iribarne, B.A. Thomson, On the evaporation of small ions from charged droplets, Journal of chemical physics, 64 (1976) 2287–2294.

[20] E. Uggerud, S. Petrie, D.K. Bohme, F. Turecek, D. Schroder, H. Schwarz, D. Plattner, T. Wyttenbach, M.T. Bowers, P.B. Armentrout, S.A. Truger, T. Junker, G. Suizdak, M. Bronstrup, Topics in Current Chemistry: Modern Mass Spectrometry, Springer-Verlag, Berlin, 2003, pp: 1-302.

[21] V.H. Wysocki, K.A. Resing, Q. Zhang, G. Cheng, Mass spectrometry of peptides and proteins, Methods, 35 (2005) 211-222.

[22] S.D. Hanton, Mass spectrometry of polymers and polymer surfaces, Chemical reviews, 101 (2001) 527-569.

[23] P. Kebarle, U.H. Verkerk, Electrospray: from ions in solution to ions in the gas phase, what we know now, Mass spectrometry reviews, 28 (2009) 898-917.

[24] M. Wilm, Principles of electrospray ionization, Molecular & cellular proteomics, 10 (2011) M111 009407.

[25] R.E. March, Quadrupole ion trap mass spectrometry: a view at the turn of the century, International journal of mass spectrometry, 200 (2000) 285-312.

[26] M. Libarondi, J. Binkley, Comparing the capabilities of time-of-flight and quadrupole mass spectrometers, Spectroscopy, (2010) Special issues.

[27] P.E. Miller, B.M. Denton, The quadruple mass filter: basic operating concepts, Journal of chemical education, 63 (1986) 617-623.

[28] C. Steel, M. Henchman, The quadruple mass filter: basic operating concepts, Journal of chemical education, 75 (1998) 1049-1054.

[29] R.J. Cotter, Peer reviewed: the new time-of-flight mass spectrometry, Analytical chemistry, 71 (1999) 445A-451A.

[30] I.V. Chernushevich, A.V. Loboda, B.A. Thomson, An introduction to quadrupole-time-of-flight mass spectrometry, Journal of mass spectrometry, 36 (2001) 849-865.

[31] J. Reinders, U. Lewandrowski, J. Moebius, Y. Wagner, A. Sickmann, Challenges in mass spectrometry-based proteomics, Proteomics, 4 (2004) 3686-3703.

[32] J. Hirsch, K.C. Hansen, A.L. Burlingame, M.A. Matthay, Proteomics: current techniques and potential applications to lung disease, American journal of physiology. Lung cellular and molecular physiology, 287 (2004) L1-23.

[33] k. Neetu, G. Ankit, T. Ruchi, B. Ajay, B. Prashant, A review on mass spectrometry detectors, International research journal of pharmacy, 3 (2012) 33-42.

[34] J.L. Wiza, Mirochannel plate detectors, Nuclear instruments and methods in physics research, 162 (1979) 587-601.

[35] J. Adams, B.W. Manley, The mechanism of channel electron multiplication, IEEE transactions on nuclear science, 13 (1966) 88-99.

[36] G. Eschard, B.W. Manley, Principle and characteristics of channel electron multipliers, Acta electronica, 14 (1971) 19-39.

[37] P. Schagen, Advances in Image Pickup and Display, Academic Press, New York, 1974 pp: 15.

[38] E.d. Hoffmann, Special feature: tutorial tandem mass spectrometry: a primer, Journal of mass spectrometry, 31 (1996) 129-137.

[39] L. Sleno, D.A. Volmer, Ion activation methods for tandem mass spectrometry, Journal of mass spectrometry, 39 (2004) 1091-1112.

[40] D. Gordon, D.R. Little, A. Farooq, Mass spectrometer and method of mass spectrometry, Patents US8598512 B2, (2013).

[41] I.V. Chernushevich, Eur. Duty cycle improvement for a quadrupole-time-of-flight mass spectrometer and its use for precusor ion scans, Mass spectrometry, 6 (2000) 471-479.

[42] J.H. Gross, Mass Spectrometry: A Textbook, Second Edition, Duty Cycle, springer-verlag, Heidelberg, Germany, 2011, pp: 134.

[43] J.E.P. Syka, J.J. Coon, M.J. Schroeder, J. Shabanowitz, D.F. Hunt, Peptide and protein sequence analysis by electron transfer dissociation mass spectrometry, Proceedings of the national academy of sciences of the USA, 101 (2004) 9528–9533.

[44] J.M. Wells, S.A. McLuckey, Collision-induced dissociation (CID) of peptides and proteins, Methods in enzymology, 402 (2005) 148-185.

[45] O.D. Sparkman, Z.E. Penton, F.G. Kiston, Gass Chromotography and Mass Spectrometry, A Practical Guide, Second Eddition, Elsevier Inc, Oxford, OX51GP, UK, 2011, pp: 423.

[46] K. Levsen, Fundamental Aspects of Organic Mass Spectroscopy, Verlag Chemie: Weinheim, New York, 1978, pp: 92 (energy dependence), 138 (collision process).

[47] P.B. Armentrout, Threshold collision-induced dissociations for the determination of accurate gas-phase binding energies and reaction barriers, Modern mass spectrometry, 225 (2003) 233-262.

[48] K. Vékey, Internal energy effects in mass spectrometry, Journal of mass spectrometry, 31 (1996) 445-463.

[49] V. Gabelica, E. De Pauw, Internal energy and fragmentation of ions produced in electrospray sources, Mass spectrometry reviews, 24 (2005) 566-587.

[50] A. Kuki, G. Shemirani, L. Nagy, B. Antal, M. Zsuga, S. Keki, Estimation of activation energy from the survival yields: fragmentation study of leucine enkephalin and polyethers by tandem mass spectrometry, Journal of the amercian society for mass spectrometry, 24 (2013) 1064-1071.

[51] S.A. McLuckey, Principles of collisional activation in analytical mass spectrometry, Journal of the American Society for Mass Spectrometry, 3 (1992) 599-614.

[52] K.L. Busch, G.L. Glish, S.A. McLuckey, Mass Spectrometry: Techniques and Applications of Tandem Mass Spectrometry, Wiley-VCH Verlag GmbH, Weinheim, 1989, pp: 64 (E_{com}), 84 (pressure effects).

[53] J.J. Manappallil, Basic Dental Materials, Second Edition, Jaypee Brothers Medical Publisher (P), MO 63043, USA, 2003, pp: 75.

[54] G. Pruckmayr, P. Dreyfuss, D.M. P., Polyethers, tetrahydrofuran and oxetane polymers KirkOthmer Encyclopedia of Chemical Technology, John Wiley & Sons, Inc. , (1996).

[55] G.P. Speranza, S.D. Lesesne, Method for preparing basic polyether compositions, in: US3110732 A, Patent, United States, 1963.

[56] M.L. Adams, A. Lavasanifar, G.S. Kwon, Amphiphilic block copolymers for drug delivery, Journal of pharmaceutical sciences, 92 (2003) 1343-1355.

[57] R. Mencucci, E. Favuzza, U. Menchini, Assessment of the tolerability profile of an ophthalmic solution of 5% glycyrrhizin and copolymer PEG/PPG on healthy volunteers and evaluation of its efficacy in the treatment of moderate to severe blepharitis, Clinical ophthalmology, 7 (2013) 1403-1410.

[58] R.M. Nalbandian, R.L. Henry, H.S. Wilks, Artificial skin. II. Pluronic F-127 Silver nitrate or silver lactate gel in the treatment of thermal burns, Journal of biomedical materials research, 6 (1972) 583-590.

[59] M. Yokoyama, Block copolymers as drug carriers, Critical reviews in therapeutic drug carrier systems, 9 (1992) 213-248.

[60] J.C. Gilbert, J. Hadgraft, A. Bye, L.G. Brooks, Drug release from Pluronic F-127 gels, International journal of pharmaceutics, 32 (1986) 223-228.

[61] M. Ionescu, Oligo-Polyols for Elastic Polyurethane in Chemistry and Technology of Polyols for Polyurethanes, Rapra Technology Limited, Shawbury, shrewsbury, Shropshire, SY4 4NR, 2005 pp: 55-155.

[62] W. Wang, X. Yang, Y. Fang, J. Ding, J. Yan, Preparation and thermal properties of polyethylene glycol/expanded graphite blends for energy storage, Journal of applied energy, 86 (2009) 1479-1483.

[63] C. Fruijtier-Polloth, Safety assessment on polyethylene glycols (PEGs) and their derivatives as used in cosmetic products, Toxicology, 214 (2005) 1-38.

[64] S. Muschert, F. Siepmann, B. Leclercq, B. Carlin, J. Siepmann, Drug release mechanisms from ethylcellulose: PVA-PEG graft copolymer-coated pellets, European journal of pharmaceutics and biopharmaceutics : official journal of Arbeitsgemeinschaft fur Pharmazeutische Verfahrenstechnik e.V, 72 (2009) 130-137.

[65] J. Kopecek, Hydrogel biomaterials: a smart future?, Biomaterials, 28 (2007) 5185-5192.

[66] Y.H. Wu, Q. Zhou, T. Zhao, M.L. Deng, J. Zhang, Y.Z. Wang, Poly(ethylene glycol) enhanced dehydrochlorination of poly(vinyl chloride), Journal of hazardous materials, 163 (2009) 1408–1411.

[67] C.W. S., M. Cho, J. Jeong, M. Choi, H.Y. Cho, B.S. Han, S.H. Kim, H.O. Kim, Y.T. Lim, B.H. Chung, J. Jeong, Acute toxicity and pharmacokinetics of 13 nm-sized PEG-coated gold nanoparticles, Journal of toxicology and applied pharmacology, 236 (2009) 16-24.

[68] E.T. Chiang, S.M. Camp, S.M. Dudek, M.E. Brown, P.V. Usatyuk, O. Zaborina, J.C. Alverdy, J.G. Garcia, Protective effects of high-molecular weight polyethylene glycol (PEG) in human lung endothelial cell barrier regulation: role of actin cytoskeletal rearrangement, Microvascular research, 77 (2009) 174-186.

[69] W.E. Barton, A.J. Daugulis, Evaluation of solvents for extractive butanol fermentation with Clostridium acetobutylicum and the use of poly(propylene glycol) 1200, Applied microbiology and biotechnology, 36 (1992) 632-639.

[70] G.I. Konishi, Y. Chujo, Synthesis of a star-shaped polymer by coordination of 2,2'-bipyridyl-terminated poly(propylene glycol) with ruthenium ion, Polymer bulletin, 43 (1999) 9-12.

[71] X. Hu, A. Fukutani, X. Liu, K. Kimbara, F. Kawai, Isolation of bacteria able to grow on both polyethylene glycol (PEG) and polypropylene glycol (PPG) and their PEG/PPG dehydrogenases, Applied microbiology and biotechnology, 73 (2007) 1407-1413.

[72] G. Shemirani, A. Kuki, L. Nagy, T. Nagy, M. Zsuga, S. Keki, Electrospray ionization tandem mass spectrometry of the star-shaped propoxylated diethylenetriamine polyols, Journal of mass spectrometry, (2015).

[73] A.K. Bhowmick, H.L. Stephens, Handbook of Elastomers Second Edition, Marcel Dekker, New York, 2000 pp: 723-734.

[74] N. Sakly, T. Touzi, H. Ben Ouadab, J. Jaffrezic-Renault, E. Marie, Y. Chevalier, Electrical characterization of a new polymeric ion-exchanging membrane for the chemical detection of anions, Materials science and engineering, 21 (2002) 15-23.

[75] J.H. Chen, J. Wei, C.Y. Chang, R.F. Laiw, Y.D. Lee, Studies on segmented polyetherurethane for biomedical application: effects of composition and hard-segment content on biocompatibility, Journal of biomedical materials research, 41 (1998) 633-648.

[76] D.J. Martin, L.A. Warren, P.A. Gunatillake, S.J. McCarthy, G.F. Meijs, K. Schindhelm, Polydimethylsiloxane/polyether-mixed macrodiol-based polyurethane elastomers: biostability, Biomaterials, 21 (2000) 1021-1029.

[77] R.E. Solis-Correa, R. Vargas-Coronado, M. Aguilar-Vega, J.V. Cauich-Rodriguez, J.S. Roman, A. Marcos, Synthesis of HMDI-based segmented polyurethanes and their use in the manufacture of elastomeric composites for cardiovascular applications, Journal of biomaterials science. Polymer edition, 18 (2007) 561-578.

[78] J.D. Fromstein, K.A. Woodhause, Polyurethane Biomaterials, Informa Healthcare Inc, New York, 2008 pp: 2304–2313.

[79] A. Kuki, L. Nagy, A. Memboeuf, L. Drahos, K. Vekey, M. Zsuga, S. Keki, Energy-dependent collision-induced dissociation of lithiated polytetrahydrofuran: effect of the size on the fragmentation properties, Journal of the american society for mass spectrometry, 21 (2010) 1753-1761.

[80] A. Kuki, L. Nagy, G. Shemirani, A. Memboeuf, L. Drahos, K. Vekey, M. Zsuga, S. Keki, A simple method to estimate relative stabilities of polyethers cationized by alkali metal ions, Rapid communications in mass spectrometry, 26 (2012) 304-308.

[81] D. Marquardt, An algorithm for least-squares estimation of nonlinear parameters, SIAM Journal of applied mathematics, 11 (1963) 431-441.

[82] K. Tanaka, H. Waki, Y. Ido, S. Akita, Y. Yoshida, T. Yohida, Protein and polymer analyses up to m/z 100,000 by laser ionization time-of-flight mass spectrometry, Rapid communications in mass spectrometry, 2 (1988) 151-153.

[83] S.F. Wong, C.K. Meng, J.B. Fenn, Multiple charging in electrospray ionization of polyethylene glycols, Journal of physical chemistry, 92 (1988) 546-550.

[84] K. Shimada, S. Matsuyama, T. Saito, S. Kinugasa, R. Nagahata, S. Kawabata, Conformational effects on cationization of poly(ethylene glycol) by alkali metal ions in matrix-assisted laser desorption /ionization time of flight mass spectrometry, International Journal of Mass Spectrometry, 247 (2005) 85.

[85] Y. Wang, H. Rashidzadeh, B. Guo, Structural effects on polyether cationization by alkali metal ions in matrix-assisted laser desorption/ionization, Journal of the American Society for Mass Spectrometry, 11 (2000) 639-643.

[86] S. Keki, L.S. Szilagyi, G. Deak, M. Zsuga, Effects of different alkali metal ions on the cationization of poly(ethylene glycol)s in matrix-assisted laser desorption/ionization mass spectrometry: a new selectivity parameter, Journal of mass spectrometry, 37 (2002) 1074-1080.

[87] A.R. Hortal, P. Hurtado, B. Martinez-Haya, A. Arregui, L. Banares, Solvent-free MALDI investigation of the cationization of linear polyethers with alkali metals, Journal of physical chemistry. B, 112 (2008) 8530-8535.

[88] M.J. Bogan, G.R. Agnes, Poly(ethylene glycol) doubly and singly cationized by different alkali metal ions: relative cation affinities and cation-dependent resolution in a quadrupole ion trap mass spectrometer, Journal of the American Society for Mass Spectrometry, 13 (2002) 177-186.

[89] S. Keki, L. Nagy, G. Deak, M. Zsuga, Multiple charging of poly(propylene glycol) by binary mixtures of cations in electrospray, Journal of the American Society for Mass Spectrometry, 16 (2005) 152-157.

[90] P.B. Armentrout, Cation-Ether complexes in the gas phase: thermodynamic insight into molecular recognition, International journal of mass spectrometry, 193 (1999) 227-240.

[91] M.B. More, D. Ray, P.B. Armentrout, Cation‑Ether complexes in the gas phase: bond dissociation energies of Na+(dimethyl ether)x, x = 1 ‑ 4; Na+(1,2‑dimethoxyethane)x, x = 1 and 2; and Na+(12-crown-4), Jourlnal of physical chemistry A, 101 (1997) 831-839.

[92] M.W. Forbes, D.A. Volmer, G.J. Francis, D.K. Bohme, A comparison of data analysis methods for determining gas phase stabilities by CID: alkali metal complexes of polyether

ionophore antibiotics, Journal of the American Society for Mass Spectrometry, 16 (2005) 779-791.

[93] E.C. Kempen, J.S. Brodbelt, R.A. Bartsch, Y. Jang, J.S. Kim, Investigation of alkali metal cation selectivities of lariat ethers by electrospray ionization mass spectrometry, Journal of analytical chemistry, 71 (1999) 5493-5500.

[94] D.S. Young, H.Y. Hung, L.K. Liu, Estimation of selectivities and relative cationization efficiencies of different [crown plus M](+) by electrospray mass spectrometry, Journal of mass spectrometry, 32 (1997) 432-437.

[95] J. Gidden, T. Wyttenbach, A.T. Jackson, J.H. Scrivens, M.T. Bowers, Gas-phase conformations of synthetic polymers: poly(ethylene glycol), poly(propylene glycol), and poly(tetramethylene glycol), Journal of the American Chemical Society, 122 (2000) 4692-4699.

[96] A. Memboeuf, K. Vekey, G. Lendvay, Structure and energetics of poly(ethylene glycol) cationized by Li(+), Na(+), K(+) and Cs(+): a first-principles study, European journal of mass spectrometry, 17 (2011) 33-46.

[97] M.R. Mauk, A.G. Mauk, Y.L. Chen, D.J. Douglas, Tandem mass spectrometry of protein-protein complexes: cytochrome c-cytochrome b5, Journal of the american society for mass spectrometry, 13 (2002) 59-71.

[98] Y.L. Chen, B.A. Collings, D.J. Douglas, Collision cross sections of myoglobin and cytochrome c ions with Ne, Ar, and Kr, Journal of the american society for mass spectrometry, 8 (1997) 681-687.

[99] D.J. Douglas, Applications of collision dynamics in quadrupole mass spectrometry, Journal of the american society for mass spectrometry, 9 (1998) 101-113.

[100] V.J. Nesatyy, J. Laskin, Dissociation of noncovalent protein complexes by triple quadrupole tandem mass spectrometry: comparison of Monte Carlo simulation and experiment, International journal of mass spectrometry, 36 (2002) 237-263.

[101] L. Drahos, K. Vekey, MassKinetics: a theoretical model of mass spectra incorporating physical processes, reaction kinetics and mathematical descriptions, Journal of mass spectrometry, 36 (2001) 237-263.

[102] J. Sztaray, A. Memboeuf, L. Drahos, K. Vekey, Leucine enkephalin--a mass spectrometry standard, Mass spectrometry reviews, 30 (2011) 298-320.

[103] F. Muntean, P.B. Armentrout, Guided ion beam study of collision-induced dissociation dynamics: integral and differential cross sections, The journal of chemical physics, 115 (2001) 1213-1228.

[104] C.M. Lock, E.W. Dyer, Simulation of ion trajectories through a high pressure radio frequency only quadrupole collision cell by SIMION 6.0, Rapid communications in mass spectrometry, 13 (1999) 422-431.

[105] T. Baer, P.M. Mayerfn, Statistical Rice-Ramsperger-Kassel-Marcus quasiequilibrium theory calculations in mass spectrometry, Journal of the american society for mass spectrometry, 8 (1997) 103-115.

[106] L. Drahos, K. Vékey, Determination of the thermal energy and its distribution in peptides, Journal of the american society for mass spectrometry, 10 (1999) 323-328.

[107] J.W. Hager, A new linear ion trap mass spectrometer, Rapid communications in mass spectrometry, 16 (2002) 512-526.

[108] A. Memboeuf, L. Drahos, K. Vekey, G. Lendvay, Energetics of fragmentation for cationized poly(ethylene glycol) oligomers, Rapid communications in mass spectrometry, 24 (2010) 2471-2473.

[109] A. Kuki, L. Nagy, T. Nagy, M. Zsuga, S. Keki, Arm-length distribution in four-arm star-propoxylated ethylenediamine polyol by tandem mass spectrometry, Journal of mass spectrometry, 48 (2013) 1125-1127.

9. PUBLICATIONS

Publications related to the dissertation:

Ghazaleh Shemirani, Ákos Kuki, Lajos Nagy, Tibor Nagy, Miklós Zsuga, Sándor Kéki. Electrospray ionization tandem mass spectrometry of the star-shape propoxylated diethylenetriamine polyols. Journal of mass spectrometry. 50 (2015) 914-917. **IF: 2.379**

Ákos Kuki, **Ghazaleh Shemirani**, Lajos Nagy, Miklós Zsuga, Sándor Kéki. Estimation of activation energies from the survival yield curves: a case study for the fragmentation of leucine enkephalin and polyethers by tandem mass spectrometry. Journal of the american society for mass spectrometry. 24 (2013) 1064-1071. **IF: 3.193**

Ákos Kuki, Lajos Nagy, **Ghazaleh Shemirani**, Antony Memboeuf, László Drahos, Károly Vékey, Miklós Zsuga, Sándor Kéki. A simple method to estimate relative stabilities of polyethers cationized by alkali metal ions. Rapid communication in mass spectrometry. 26 (2012) 304-308. **IF: 2.509**

Other publication:

Ákos Kuki, Izabella Irsai, Lajos Nagy, **Ghazaleh Shemirani**, Cornelia Majdik, Miklós Zsuga, Sándor Kéki. In-source collision induced dissociation study of polyethers cationized by alkali metal ions. International journal of mass spectrometry. 334 (2012) 38-42. **IF: 2.227**